JEM Journal of Experimental Medicine

ARTICLE

Identification of an anergic B_{ND} cell–derived activated B cell population ($B_{ND}2$) in young-onset type 1 diabetes patients

Zachary C. Stensland[1,2], Christopher A. Magera[2], Hali Broncucia[2], Brittany D. Gomez[3], Nasha M. Rios-Guzman[2,3], Kristen L. Wells[2], Catherine A. Nicholas[2,4], Marynette Rihanek[2], Maya J. Hunter[2], Kevin P. Toole[2], Peter A. Gottlieb[1,2], and Mia J. Smith[1,2,3]

Recent evidence suggests a role for B cells in the pathogenesis of young-onset type 1 diabetes (T1D), wherein rapid progression occurs. However, little is known regarding the specificity, phenotype, and function of B cells in young-onset T1D. We performed a cross-sectional analysis comparing insulin-reactive to tetanus-reactive B cells in the blood of T1D and controls using mass cytometry. Unsupervised clustering revealed the existence of a highly activated B cell subset we term $B_{ND}2$ that falls within the previously defined anergic B_{ND} subset. We found a specific increase in the frequency of insulin-reactive $B_{ND}2$ cells in the blood of young-onset T1D donors, which was further enriched in the pancreatic lymph nodes of T1D donors. The frequency of insulin-binding $B_{ND}2$ cells correlated with anti-insulin autoantibody levels. We demonstrate $B_{ND}2$ cells are pre-plasma cells and can likely act as APCs to T cells. These findings identify an antigen-specific B cell subset that may play a role in the rapid progression of young-onset T1D.

Introduction

While T cells are known to be the executioners of the insulin-producing pancreatic beta cells in type 1 diabetes (T1D), B cells are thought to have an important role in the pathogenesis of T1D. It is clear that autoantibodies produced by terminally differentiated daughters of B cells are important for early identification of individuals at increased risk for progression to T1D, yet current dogma suggests these autoantibodies are likely not pathogenic (Wong et al., 2004). Instead, studies in mice indicate the major effector function of B cells in T1D is likely through essential antigen presentation to cognate T cells (Falcone et al., 1998; Serreze et al., 1998; Silveira et al., 2002). Given the importance of B cells in T1D, many have sought to define the phenotype and function of B cells in T1D, beginning with the analysis of peripheral blood B cells by flow cytometry. However, there is no consensus regarding a unique disease-associated B cell phenotype or function; conclusions have ranged from an increase in marginal zone B cells to a decrease in regulatory B cells to no detectable disease-specific B cell phenotype (Deng et al., 2016; Kleffel et al., 2015; Powell et al., 2018; Thompson et al., 2014). It was not until recently that a consistent picture of B cell function in T1D has begun to emerge.

In a groundbreaking study by Leete et al., pancreatic B cells of organ donors were found to display two distinct patterns of insulitis depending on subject age. Subjects who were diagnosed before the age of 7 always exhibit increased numbers of B cells ($CD20^+$ cells) in the islets relative to subjects diagnosed after 13 yr of age. Furthermore, they found that subjects who display the high B cell profile (CD20Hi) show more rapid loss of beta cell mass than those with the low B cell (CD20Lo) phenotype, suggesting the two forms of disease are differentially aggressive (Leete et al., 2016). More recently, this difference in age-associated B cell numbers was supported in two separate studies that analyzed rate of C-peptide loss, an indicator of reduced beta cell function, and variations in gene expression in new-onset T1D subjects. Both studies concluded that rapid loss in C-peptide is restricted to young-onset subjects and is associated with increased expression of B cell genes, consistent with increased B cell numbers determined by flow cytometry (Dufort et al., 2019; Speake et al., 2019). Despite clear evidence for B cell involvement in the young-age-associated aggressive form of T1D, previous studies have been limited to a description of a generalized B cell phenotype, i.e., an increase in total B cells in

[1]Department of Pediatrics, University of Colorado School of Medicine, Aurora, CO, USA; [2]Barbara Davis Center for Diabetes, University of Colorado School of Medicine, Aurora, CO, USA; [3]Department of Immunology and Microbiology, University of Colorado School of Medicine, Aurora, CO, USA; [4]Department of Biochemistry and Molecular Genetics, University of Colorado School of Medicine, Aurora, CO, USA.

Correspondence to Mia J. Smith: mia.smith@cuanschutz.edu.

young-onset T1D. Hence, knowledge of which B cell subset, including its antigen specificity, activations status, and mechanism of action that contributes to development of T1D is currently unknown. Such information is vital to understanding the pathogenesis of disease in the two endotypes of T1D and development of proper age-appropriate interventions and therapies to prevent and treat disease.

In healthy individuals, autoreactive B cells are silenced by one of three mechanisms: receptor editing, clonal deletion, or anergy (Smith et al., 2017). Both receptor editing and clonal deletion occur centrally in the bone marrow, whereas anergy typically occurs in the periphery. Autoreactive anergic B cells are characterized by a state of unresponsiveness. In the classical model of anergy, autoreactive B cells are rendered unresponsive as a consequence of chronic receipt of signal 1 (antigen recognition through the B cell receptor [BCR]) without signal 2 (cognate T cell help). Chronic stimulation by self-antigen imposes unresponsiveness by downregulation of BCR, primarily IgM, and activation of negative regulatory signaling molecules, such as PTEN and SHIP-1 (Cambier et al., 2007; Duty et al., 2009; Gauld et al., 2005; Gauld et al., 2006; Getahun et al., 2016). Anergic B cells have been shown to undergo follicular exclusion and have a shortened half-life (Cyster and Goodnow, 1995). Importantly, studies in mice demonstrate that anergy is reversible, and therefore, when anergy is breached, possibly through receipt of cognate T cell help (signal 2) and TLR stimulation (signal 3), and/or alterations in inhibitory receptor signaling, autoimmunity can ensue (Gauld et al., 2005; Smith et al., 2019; Smith et al., 2018a).

Hypothesizing that maintenance of B cell anergy in self-reactive B cells is impaired during development of T1D, we previously analyzed the frequency of anergic (naive IgD^+ B cell [B_{ND}]) insulin-binding B cells in the peripheral blood of subjects along a continuum of diabetes development. We showed that new-onset, autoantibody-positive first-degree relatives (FDRs), and some autoantibody-negative FDRs exhibit a loss of high affinity anergic (B_{ND}) insulin-reactive B cells in their peripheral blood relative to long-standing T1D and healthy controls (Smith et al., 2015). In a follow-up study, we demonstrated that loss of anergic insulin-reactive B cells in autoantibody negative FDRs was associated with high-risk HLA (i.e., DR4-DQ8) and non-HLA T1D risk alleles (e.g., INS, PTPN2; Smith et al., 2018b). Loss of B_{ND} cells may reflect a phenotypic change or actual departure from peripheral blood.

Based on our previous findings, we posit that loss of anergic insulin-reactive B cells in the peripheral blood seen in recently diagnosed T1D and autoantibody-positive FDRs reflects their activation and/or acquisition of the capacity to participate in the pathogenesis of T1D through antigen presentation to T cells, production of cytokines, and/or production of autoantibodies. To test this hypothesis and to identify the diabetogenic B cell operative in young-onset T1D, we used mass cytometry to more deeply phenotype the peripheral B cell compartment in these individuals compared with teen-onset, adult-onset, and age-matched controls on an antigen-specific level. We identified a specific expansion of activated insulin-reactive B cells in the previously defined anergic B_{ND} subset (Duty et al., 2009) in young-onset T1D donors that is not present in older-onset T1D subjects. We term these cells $B_{ND}2$. Phenotypically these cells resemble anergic B cells in that they are $CD27^-$ IgD^+ $IgM^{lo/-}$; however, they express markers of activation, including CD69, CD86, CD95, and CD11c. In addition, $B_{ND}2$ cells also lack expression of CD21 and CXCR5, appearing somewhat similar to the double negative (DN; $CD27^-$ IgD^-) B cell subset, called DN2 (Jenks et al., 2018). DN2 cells have been previously reported to be class-switched (IgG^+), extrafollicular ($CXCR5^-$), enriched in autoreactivity, precursors to antibody-secreting cells (ASCs), and are increased in subjects with systemic lupus erythematosus (SLE), rheumatoid arthritis (RA), and primary Sjogren's syndrome (pSS; Cowan et al., 2020; Jenks et al., 2018; Moura et al., 2017; Saadoun et al., 2013).

Importantly, in our study, we found $B_{ND}2$ cells are enriched in insulin reactivity and the frequency of insulin-reactive $B_{ND}2$ cells correlated with levels of anti-insulin antibodies in T1D subjects, while neither association is seen with the DN2 subset. Furthermore, we show that insulin-binding $B_{ND}2$ cells are enriched in the pancreatic lymph nodes (pLN) of T1D organ donors. They express markers consistent with capacity to act as potent APCs and ability to differentiate into ASCs in vitro. Finally, we show that classic anergic B cells can be induced to differentiate into $B_{ND}2$ cells by stimulation with a combination of CD40L, IL-21, and TLR7. Thus, we identify an islet-antigen reactive B cell subset that is specifically increased in the blood and pLN of young-onset T1D donors and suggest a mechanism of action by which $B_{ND}2$ cells could contribute to the rapid progression of disease seen in this age group. An increase of insulin-reactive $B_{ND}2$ cell frequency in the blood could serve as a biomarker for increased risk of early-onset T1D and these cells may be a target for clinical intervention studies.

Results

Identification of the unique activated B cell subset $B_{ND}2$ in total peripheral blood B cells using mass cytometry

To define the diabetogenic B cell operative in the pathogenesis of T1D, we utilized high dimensional single-cell mass cytometry (cytometry time of flight [CyTOF]) to deeply phenotype the B cell compartment using an in-depth B cell–focused antibody panel (Table S1). This 38-marker panel allows for identification of the major B cell subsets currently known, as well as their activation status, inhibitory receptor expression level, and potential in vivo function. Importantly, we also combined enrichment of insulin-reactive and tetanus-reactive B cells from peripheral blood to compare islet-reactive to foreign-reactive B cell phenotypes. Enrichment was achieved using our previously described antigen-reactive B cell enrichment method, which is compatible with mass cytometry (Stensland and Smith, 2021). For this study, we recruited 38 recently diagnosed (<100 d) T1D patients (age: 16.5 ±9.1 [mean ± SD]) and 40 healthy controls (HC; age: 17.0 ± 10.3 [mean ± SD]; Table 1 and Table S2). Irrespective of their antigen reactivity, enriched insulin, and tetanus-reactive $CD19^+$, B cells were first characterized using unsupervised clustering to identify major B cell subpopulations among T1D and HC donors (Fig. 1 A). Using this approach, we

Table 1. **Study participant demographics stratified by age**

Subjects (*n*)	Age (mean ± SD)	Sex (% F)	Race/Ethnicity (%)	% FDR
Young-onset T1D (≤10 yr old; 13)	7.07 ± 2.59	25%	White (54) White, Hispanic (23) Asian (7.7) Multiple (7.7) Unknown (7.7)	N/A
Young HC (≤10 yr old; 13)	7.54 ± 2.40	38%	White (77) White, Hispanic (16) Asian (0) Multiple (0) Unknown (7)	46%
T(w)een-onset T1D (11–17 yr old; 12)	13.70 ± 1.80	58%	White (75) White, Hispanic (16.7) Asian (8.3) Multiple (0) Unknown (0)	N/A
T(w)een HC (11–17 yr old; 12)	13.5 ± 2.0	50%	White (66.7) White, Hispanic (25) Asian (0) Multiple (0) Unknown (8.3)	58%
Adult-onset T1D (≥18 yr old; 13)	25.92 ± 7.86	31%	White (70) White, Hispanic (15) Asian (0 Multiple (0) Unknown (15)	N/A
Adult HC (≥18 yr old; 15)	31.5 ± 7.74	47%	White (66.7) White, Hispanic (20) Asian (6.7) Multiple (6.7) Unknown (0)	27%

identified 12 unique B cell subsets for both the T1D and HC subjects, 11 of which were identical between groups. Unique to the T1D group was an IgD^+ memory B cell population, whereas in the HC group an IgM^+ memory B cell population was identified (cluster 6; Fig. 1 B and Fig. S1). The IgD^+ memory population in T1D subjects likely are the previously identified Cδ-CS population that has been shown to be IgD heavy chain class-switched and enriched in auto/polyreactive (including insulin-reactive) B cells (Koelsch et al., 2007).

Of the remaining identical 11 B cell subsets identified among T1D and HCs, we identified a unique $CD27^-$ B cell subset that resembled classic anergic (B_{ND}) B cells, in that it had down-regulated surface IgM but retained IgD on its cell surface (Duty et al., 2009). However, unlike B_{ND} cells, this population demonstrated increased expression of activation markers, including CD69, CD80, and CD11c, and loss of CD21 and CXCR5 expression, which is similar to DN2 cells (Fig. S1). Hence, we termed this population $B_{ND}2$ (cluster 2 in Fig. 1 B), distinguishing it from classic anergic B_{ND} cells, which we term $B_{ND}1$ (cluster 1 in Fig. 1 B). Other interesting B cell subsets identified include a $CD11c^+$ mature naive (MN; $CD27^-$ IgM^+ IgD^+ $CD11c^+$) B cell subset (cluster 3) and a $CCR4^{hi}$ $CXCR3^{hi}$ $PD\text{-}1^{hi}$ B cell subset (cluster 12; Fig. 1 B). Next, we determined whether any of the 12 B cell subsets identified are enriched in autoreactive cells, i.e., insulin reactivity. As shown in Fig. 1 C, overall the B cell subsets identified in the T1D subjects demonstrated increased frequency of insulin-reactive cells compared with the HC group, with the highest frequency detected in the $B_{ND}1$, $B_{ND}2$, and IgD-memory (Cδ-CS) populations. On the other hand, in the HC group, the $B_{ND}2$ subset showed the highest level of insulin reactivity, followed by $CD11c^+$ MN and DN2 cells (Fig. 1 C and Fig. S2). When we compared levels of tetanus reactivity among the B cell subsets, the $CD11c^+$ MN, immature, marginal zone–like memory, and IgG^+ memory B cell subsets showed the highest level of binding in both the T1D and HC groups (Fig. 1 D and Fig. S2). Overall these results support our previous findings, as well as the work of others, that B_{ND} and Cδ-CS cells are enriched in (high affinity) insulin-reactive B cells (Duty et al., 2009; Koelsch et al., 2007; Smith et al., 2015).

$B_{ND}2$ cells show evidence of recent activation and are enriched in insulin reactivity

Next, we wanted to more formally compare differences in surface marker expression among MN ($CD27^-IgM^+IgD^+$), $B_{ND}1$, $B_{ND}2$, and the phenotypically similar DN2 subset in T1D and HC. To do this, we manually gated the above B cell subsets from total $CD19^+$ B cells (Fig. 2 A), irrespective of their antigen reactivity, and quantified expression levels of surface markers from our B cell antibody panel. As shown in Fig. 2 B, compared to $B_{ND}1$ cells, $B_{ND}2$ cells had significantly higher expression levels of the

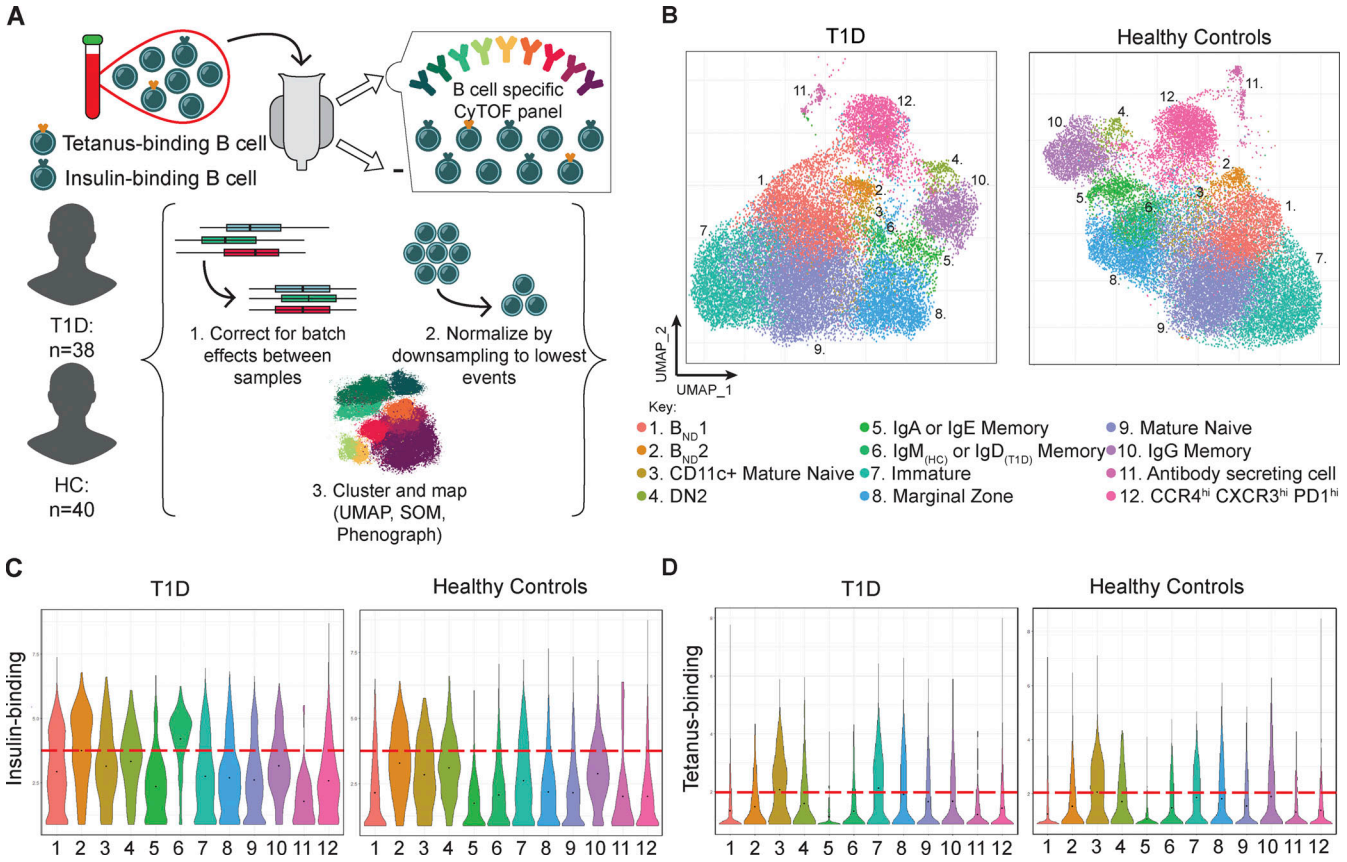

Figure 1. **Unsupervised clustering reveals novel B cell subpopulations among T1D and HC donors. (A)** Overall schematic of the study and unsupervised clustering analysis. Insulin-binding and tetanus-binding B cells were enriched from the peripheral blood of T1D (n = 38) and HC (n = 40) donors, stained with a panel of B cell–focused antibodies, and processed for mass cytometry. **(B)** UMAP plots of B cell populations identified through clustering by surface marker expression for T1D and HC donors using mass cytometry. 12 unique B cell subsets were identified for the T1D and HC groups. IgM memory B cells were found only in HC, while IgD memory B cells were found only in T1D subjects (cluster 6). Autoreactive anergic B_{ND} cells ($CD27^-$ IgM^{lo} IgD^+) were divided into two subpopulations, $B_{ND}1$ and $B_{ND}2$, based on differences in activation markers. $B_{ND}2$ cells exhibit increased surface marker expression of CD69, CD80, CD95, and CD11c compared with $B_{ND}1$ cells. **(C)** Violin plots of insulin-binding levels for each B cell population identified for T1D and HC donors. The red dotted line indicates the cutoff for true insulin-binding versus non-binding B cells. The cutoff was determined using T cell binding and unenriched B cells as negative controls. $B_{ND}1$, $B_{ND}2$, and IgD memory B cells were enriched in insulin-reactivity in T1D subjects, while $B_{ND}2$, $CD11c^+$ MN, and DN2 cells were enriched in insulin-reactivity in HC. **(D)** Violin plots of tetanus-binding levels for each B cell population for comparison to insulin-binding levels.

following activation markers: CD69, CD86, CD80, CD95, and CD11c. Moreover, $B_{ND}2$ cells showed decreased expression of CD23 and CD40, which likely reflects recent activation (Pignarre et al., 2021). Interestingly, while $B_{ND}2$ cells showed a slight decrease in HLA-DR levels compared with $B_{ND}1$ cells, their levels were significantly higher compared with DN2 cells, suggesting $B_{ND}2$ cells may retain the capacity to act as APCs. In addition, $B_{ND}2$ cells demonstrated significantly higher levels of the inhibitory receptors CD72 and CD22 compared with DN2 cells (Fig. 2 B). Next, we compared the expression of known surface markers present on plasmablasts and/or plasma cells. $B_{ND}2$ cells expressed significantly less CD71, CXCR3, CD138, and CD38 compared with manually gated plasmablasts. Interestingly, $B_{ND}2$ levels of CD71 and CD38 trended higher or were significantly higher than $B_{ND}1$ and DN2 cells (Fig. 2 C). When we compared surface marker expression for all of the above markers between HC and T1D donors, the only significant difference found was in expression of CD69, which was significantly higher in the $B_{ND}2$ cells in T1D compared with HC (*P < 0.05).

Given our findings in Fig. 1 that $B_{ND}2$ cells were enriched in insulin-reactive cells, we next quantified the percent of insulin-reactive B cells among MN, $B_{ND}1$, $B_{ND}2$, DN2, and plasmablasts (PB). We found that both $B_{ND}1$ and $B_{ND}2$ subsets were enriched in insulin-reactive B cells in both the T1D and HC donors, which was significantly increased compared with DN2 and PB (Fig. 2 D). When we compared the frequency of tetanus-reactive B cells among the various B cell subsets, we found no significant differences, demonstrating selective self-reactivity among the B_{ND} subsets. Lastly, given that DN2 cells have been shown previously to be IgG^+ class-switched B cells that lack expression of the canonical memory B cell marker, CD27, we wondered whether $B_{ND}2$ cells also expressed membrane IgG. We found that the $B_{ND}2$ population contained significantly fewer IgG-expressing B cells than DN2 cells or plasmablasts, but were increased compared with $B_{ND}1$ cells (Fig. 2 E). Given that $B_{ND}2$ cells express high amounts of IgD on their cell surface, we hypothesize coexpression of surface IgD and IgG on $B_{ND}2$ cells likely reflects early evidence of class-switching to IgG, with continued

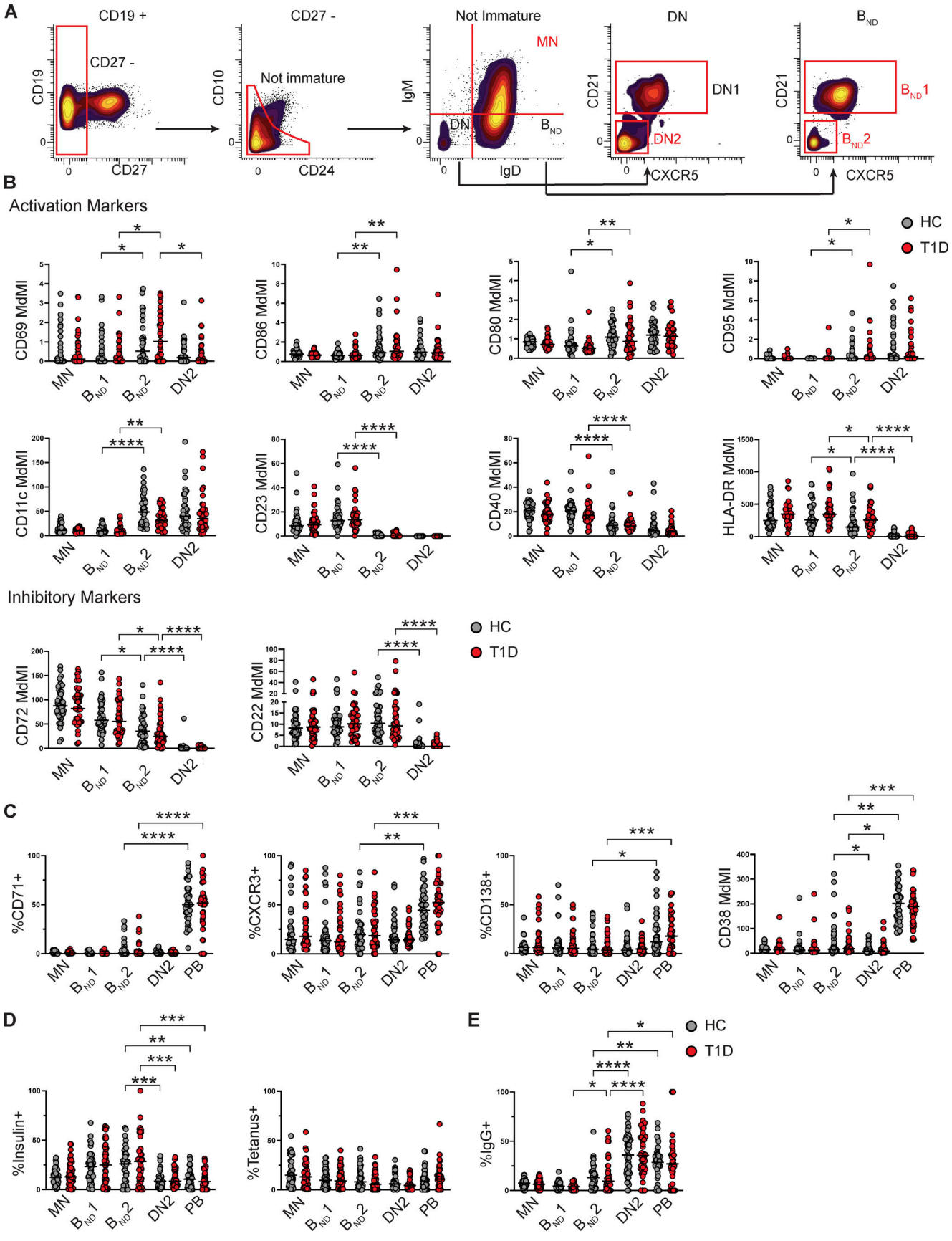

Figure 2. **Surface marker expression of $B_{ND}2$ cells demonstrates these cells are recently activated and enriched in insulin reactivity. (A)** Manual gating scheme for identification of MN, $B_{ND}1$, $B_{ND}2$, and DN2 populations. **(B)** Comparison of surface marker expression levels of various activation and inhibitory

molecules for MN, $B_{ND}1$, $B_{ND}2$, and DN2. Antibody staining intensity is represented as median metal intensity (MdMI). $B_{ND}2$ cells exhibit significantly increased expression of markers of activation compared to $B_{ND}1$ cells, which is similar to DN2 cells. $B_{ND}2$ cells maintain surface expression of the inhibitory receptors CD72 and CD22 compared with DN2 cells. **(C)** Comparison of $B_{ND}2$ cells with surface markers associated with PB/plasma cells. $B_{ND}2$ cells have significantly reduced levels of markers associated with PB/plasma cells but are increased in expression of CD71 and CD38 compared with DN2 cells. PB were gated as $CD19^+$ CD38hi CD27hi. **(D)** Comparison of the frequency of insulin- and tetanus-positive B cells among various B cell subsets. $B_{ND}1$ and $B_{ND}2$ cells are enriched in insulin reactivity, but not tetanus reactivity, compared with DN2 cells. **(E)** Comparison of the frequency of IgG^+ B cells among the various B cell subsets. $B_{ND}2$ cells have increased expression of surface IgG compared to $B_{ND}1$ cells but is decreased compared with DN2 cells. Data generated from T1D (n = 38) and HC (n = 40) donors. Statistical significance determined by mixed-effects model. *P < 0.05, **P < 0.01, ***P < 0.001, ****P < 0.0001.

detection of IgD on the cell surface due to long BCR half-life. In line with this, the expression of IgD on IgG^+ $B_{ND}2$ cells is significantly less than the expression of IgD on IgG^- $B_{ND}2$ cells (data not shown).

The frequency and absolute number of insulin-binding $B_{ND}2$ cells are increased in young-onset T1D donors and correlate with insulin-autoantibody levels

Given the numerous conflicting reports that have sought to identify differences in B cell subset frequencies in T1D versus HC subjects, we next wanted to analyze the difference in frequency of all major B cell subsets, including those identified using the unbiased approach employed in Fig. 1 B, on an antigen-specific level and in age-stratified groups. We gated on insulin- or tetanus-reactive B cells among $CD19^+$ B cells in our magnetically enriched fraction (Fig. 3 A) and analyzed the frequency of various B cell subsets across three age groups: (1) recently diagnosed T1D and HC subjects ≤10 yr old, (2) 11–17 yr old, and (3) 18 yr old and over (Table 1). We found a significant increase in the frequency and absolute number of insulin-binding $B_{ND}2$ cells in young-onset (≤10 yr old) T1D compared with the 18+ T1D, and a significant increase in the frequency and trend in absolute number (P = 0.078) in the insulin-binding $B_{ND}2$ cells in the ≤10 yr old T1D compared with the 11–17 age groups. Importantly, there was no increase in the frequency or absolute number of tetanus-reactive $B_{ND}2$ cells in the ≤10 T1D group, demonstrating the islet-antigen specificity of this finding (Fig. 3, B and C). Given previous studies demonstrating that the frequency of DN2 cells is increased in SLE, RA, and pSS subjects, we next wondered whether DN2 cells were also increased in T1D subjects. As shown in Fig. 3, D and E, we found no significant increase in insulin- or tetanus-reactive DN2 cells in any of our T1D age groups. We also analyzed the frequency of antigen-reactive cells in other major B cell subsets, including immature, naive, memory, IgG^+ class-switched, IgG^- class-switched, PB, B10 (enriched in B regulatory cells), and the $CXCR3^{hi}$ $CCR4^{hi}$ population identified in our unsupervised clustering, and found no significant difference in frequencies among our T1D age groups compared with age-matched controls (data not shown). Hence, in this study, the only significant difference found among the three T1D age groups was the frequency of insulin-reactive $B_{ND}2$ cells.

Given that $B_{ND}2$ cells express some PB markers and the phenotypically similar DN2 subset has previously been shown to be precursors to ASCs, we wondered whether the frequency of insulin-binding $B_{ND}2$ and/or DN2 cells correlated with levels of anti-insulin autoantibodies in our T1D subjects. We found a strong and significant correlation between the frequency of insulin-binding $B_{ND}2$ cells in the peripheral blood and the levels of anti-insulin autoantibodies in our T1D subjects, irrespective of their age at diagnosis. Unlike studies in SLE, in which the frequency of DN2 cells correlated with anti-nuclear autoantibodies (Jenks et al., 2018), we saw no correlation between the frequency of insulin-binding DN2 cells and anti-insulin autoantibody levels (Fig. 3 F).

Previous studies have demonstrated that young-onset T1D subjects tend to develop autoantibodies against insulin first, followed by other islet antigens, such as GAD65 and IA-2, and tend to carry the high-risk HLA DR4-DQ8 allele (Bingley et al., 2016; Gorus et al., 2017). Hence, we next determined whether individuals carrying the high-risk HLA DR4-DQ8 allele also contain the highest frequency of insulin-binding $B_{ND}2$ cells in their blood. Indeed, we found that individuals who had the highest frequency of insulin-binding $B_{ND}2$ cells also carried the HLA DR4-DQ8 allele (Fig. 3 G). On the other hand, HCs who carried the T1D protective allele, DQ*0602, tended to have the lowest frequency of insulin-binding $B_{ND}2$ cells, suggesting this allele may also help to limit activation of insulin-reactive anergic B cells. Interestingly, in this study, there was one ≤10-yr-old HC subject who had a high level of insulin-reactive $B_{ND}2$ cells and also carried the high-risk DR4-DQ8 allele. This individual also happens to be an FDR of a T1D subject. Hence, it is tempting to speculate that this individual will progress to anti-insulin autoantibody positivity and perhaps T1D. Follow-up studies are currently in progress to assess this possibility. Also to note, if this subject is excluded from the analysis then the percent of insulin-binding $B_{ND}2$ cells in the ≤10-yr-old T1D group becomes significantly increased compared with the ≤10-yr-old HC group (*P = 0.03).

Insulin-binding $B_{ND}2$ cells expressing high levels of CD86 and CXCR3 are enriched in the pLNs of recently diagnosed T1D donors

Given that T1D is an organ-directed autoimmune disorder, we next wondered whether changes observed in the peripheral blood are reflective of what occurs near the site of autoimmune attack. To answer this question, we enriched insulin-binding B cells from freshly collected pLN from six recently diagnosed T1D cadaveric organ donors and three non-diabetic (ND) controls (Table 2) provided by the Network for Pancreatic Organ Donors (nPOD) and analyzed samples using a modified B cell flow cytometry panel. The three ND controls all carried the high-risk HLA DR4-DQ8 risk allele. We first compared differences in frequencies of various B cell subsets, including MN, $B_{ND}1$, $B_{ND}2$, DN2, and memory ($CD27^+$) B cells in the pLN, irrespective of their antigen reactivity to insulin, in T1D and ND samples. We

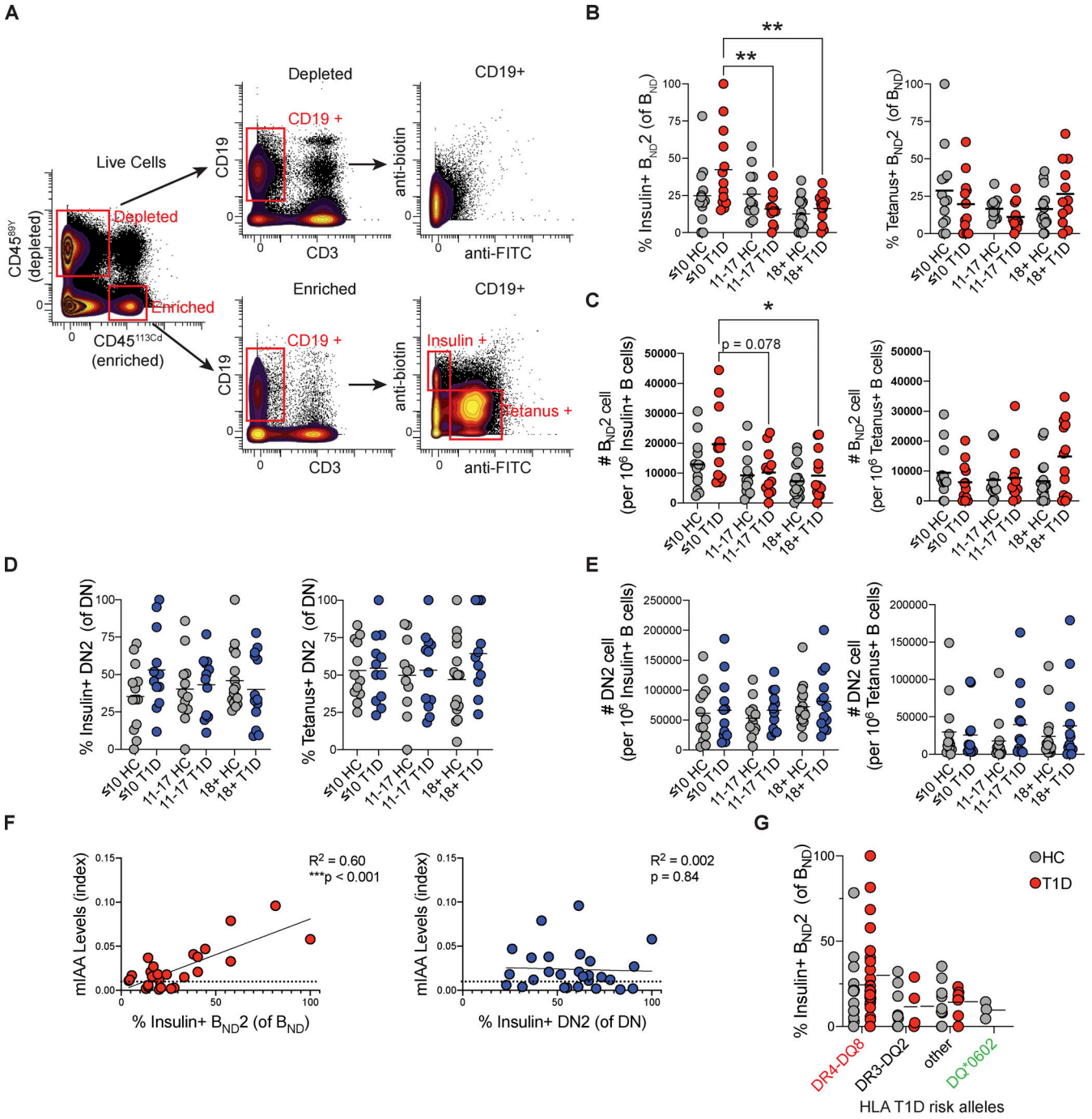

Figure 3. **Insulin-binding $B_{ND}2$ cells are increased in young-onset T1D subjects and correlate with insulin autoantibody levels. (A)** Gating strategy to determine insulin and tetanus reactivity among antigen enriched fractions. PBMCs were enriched for insulin-binding and tetanus-binding B cells simultaneously using magnetic beads. The enriched fractions were labeled with anti-CD45-113Cd, while the depleted fractions were stained with anti-CD45-89Y. Enriched and depleted fractions were combined and processed through the mass cytometer as one sample. To define/gate on insulin-binding and tetanus-binding B cells, antigen-binding levels in the enriched fraction were compared to the depleted fraction, as well as to T cells (not shown). **(B)** Insulin-binding $B_{ND}2$ cells are significantly increased in young-onset T1D (≤10 yr old; n = 12) compared with 11–17 yr old (n = 13) T1D and ≥18 yr old (n = 13) T1D groups. Insulin-binding $B_{ND}2$ cells were not increased compared to young ≤10 yr old HC (n = 13), 11–17 yr old HC (n = 12), or ≥18 yr old HC (n = 15). Tetanus-binding $B_{ND}2$ cells are not increased in young-onset T1D, demonstrating specificity of an increase in insulin-reactive B cells. Statistical significance determined by one-way ANOVA with Tukey multiple comparisons post-test. **P < 0.01. **(C)** Absolute number of insulin- and tetanus-binding $B_{ND}2$ cells in T1D and HC. *P < 0.05 **(D)** The frequency of insulin- and tetanus-binding DN2 cells were not significantly increased in the young-onset T1D group. **(E)** Absolute number of insulin- and tetanus-binding DN2 cells are not significantly different. **(F)** The frequency of insulin-binding $B_{ND}2$ cells, but not DN2 cells, in T1D subjects, irrespective of their age of onset, correlates with anti-insulin antibody titers (mIAA Levels). The black dotted line indicates cutoff value for insulin autoantibody positivity. Statistical significance determined by Spearman's Correlation, ***P < 0.001. **(G)** Increased frequency of insulin-binding $B_{ND}2$ cells is associated with carriers of the high-risk HLA-DR4-DQ8 allele (red), whereas decreased frequency of insulin-binding $B_{ND}2$ cells is associated with the T1D protective DQ*0602 allele (green). Black solid bar indicates mean for each group.

Table 2. **nPOD donors**

nPOD case ID	Donor type	Age	Diabetes duration (yr)	HLA II	% insulin-binding $B_{ND}2$ (pLN)	% insulin-binding DN2 (pLN)
6523	T1D	12	3	DR3-DQ2	57.10	90.9
6533	T1D	3	0	DR4-DQ8	60.3	76.9
6536	T1D	20	4	DR4-DQ8	13.3	30.4
6537	ND	33	-	DR4-DQ8	0	0
6548	ND	20	-	DR4-DQ8	0	0
6550	T1D	25	0	Other	45	48.1
6552	ND	33	-	DR4-DQ8	0	0
6563	T1D	14	0	Other	23	42.9
6566	T1D	15	2	DR4-DQ8	12.2	28.7

found no significant difference in the frequencies of these total B cell subsets among T1D and ND donors (data not shown). Next, we determined whether any of the above B cell subsets are enriched in insulin-reactive B cells in the pLN. As shown in Fig. 4 A, we found that $B_{ND}2$ cells were significantly enriched in insulin-reactive B cells compared to MN, $B_{ND}1$, DN2, and memory B cells in the pLN of T1D donors. Importantly, the frequency of insulin-binding B cells among the $B_{ND}2$ subset increased from around 30% in the peripheral blood to 60% in the pLN, demonstrating localization in the pLN and/or local activation of $B_{ND}1$ cells within the draining pLN of T1D donors. In line with this, unlike our findings in the peripheral blood of HC donors (Fig. 2 C), there was a significant decrease in the frequency of insulin-binding B cells among $B_{ND}2$ cells in ND controls compared with T1D donors (Fig. 4 A), suggesting that in ND controls there is a lack of trafficking to the pLN and/or lack of local activation of $B_{ND}1$ cells leading to differentiation into $B_{ND}2$ cells. While insulin-binding B cells were not as frequent among the DN2 subset as $B_{ND}2$ cells in the pLN of our T1D donors, we did find an increase in insulin-binding B cells among DN2 cells in the pLN relative to the peripheral blood (~30 vs. 10%; Fig. 4 A). This finding suggests insulin binding DN2 cells may also traffic to the pLN during T1D.

Next, given that total $B_{ND}2$ cell frequency did not differ between T1D and ND donors, we wondered whether the frequency of insulin-binding $B_{ND}2$ cells differed in T1D versus ND controls. We found that there was a significant increase in insulin-binding $B_{ND}2$ cells in T1D donors compared with ND donors, which was not found among non-insulin-binding B cells (Fig. 4 B). Similarly, insulin-binding DN2 cells were also increased in T1D relative to ND donors, which was not seen in non-insulin-binding B cells (Fig. 4 C). Given the age of onset of T1D in our T1D organ donors ranged from 3 to 25 yr old, with a mean age of 13.3 yr old, we wondered whether the youngest onset T1D organ donors had highest frequencies of insulin-binding $B_{ND}2$ and/or DN2 cells compared with older onset T1D organ donors. Indeed, the T1D donors that were youngest at onset (ages 3 and 9) both had the highest frequencies of insulin-binding $B_{ND}2$ and DN2 cells in their pLN among the six T1D organ donors (Table 2), suggesting possible participation of both insulin-binding $B_{ND}2$ and DN2 cells in the pathogenesis of young-onset T1D. Finally, we determined whether insulin-binding $B_{ND}2$ and DN2 cells in the pLN of T1D donors demonstrated evidence of recent activation and/or trafficking compared with non-insulin binding $B_{ND}2$ and DN2 cells. We found that CD86 expression was increased, though not significantly, in insulin-binding $B_{ND}2$ cells compared to non-insulin-binding $B_{ND}2$ cells, whereas levels of CD86 in DN2 cells tended to be increased, though not significantly, in non-insulin-binding DN2 cells compared with insulin-binding DN2 cells (Fig. 4 D). Overall, CD86 expression was increased in insulin-binding $B_{ND}2$ cells compared with insulin-binding DN2 cells in T1D donors (Fig. 4 E). To determine whether $B_{ND}2$ and DN2 cells show signs of recent trafficking to the pLN, we analyzed expression of the chemokine receptor CXCR3, which has been shown to be increased in islet infiltrating lymphocytes in T1D subjects (Roep et al., 2010; Sarkar et al., 2012; Uno et al., 2010). We found that insulin-binding $B_{ND}2$ and DN2 cells expressed significantly more CXCR3 than non-insulin-binding $B_{ND}2$ and DN2 cells and that the percent CXCR3-positive insulin-binding $B_{ND}2$ cells trended higher, though not significantly, compared with insulin-binding DN2 cells (Fig. 4, F and G). Overall, our findings from the pLN of T1D and ND donors demonstrate that $B_{ND}2$ cells are enriched in autoreactivity, i.e., insulin reactivity, and insulin-binding $B_{ND}2$ cells are increased in frequency in T1D donors and express increased markers of activation compared with DN2 cells. In addition, proper tolerance mechanisms appear in place in ND donors since these individuals lack insulin-binding $B_{ND}2$ and DN2 cells in their pLN.

$B_{ND}2$ cells demonstrate evidence of recent activation through their BCR, similar to DN2 cells

Given that classic anergic B cells ($B_{ND}1$) are characterized as being hyporesponsive to BCR stimulation due to chronic antigen stimulation and upregulation of inhibitory molecules, we next compared the ability of $B_{ND}2$ cells from T1D and HC donors to respond to BCR stimulation using phosflow. As shown in Fig. 5 A, irrespective of donor type, classic anergic $B_{ND}1$ cells demonstrated reduced phosphorylation of proximal BCR signaling molecules, Syk, PLCy2, and Akt, after anti-BCR stimulation compared with MN ($CD27^-$ IgM^+ IgD^+) B cells, indicative of anergy. On the other hand, $B_{ND}2$ cells demonstrate increased basal

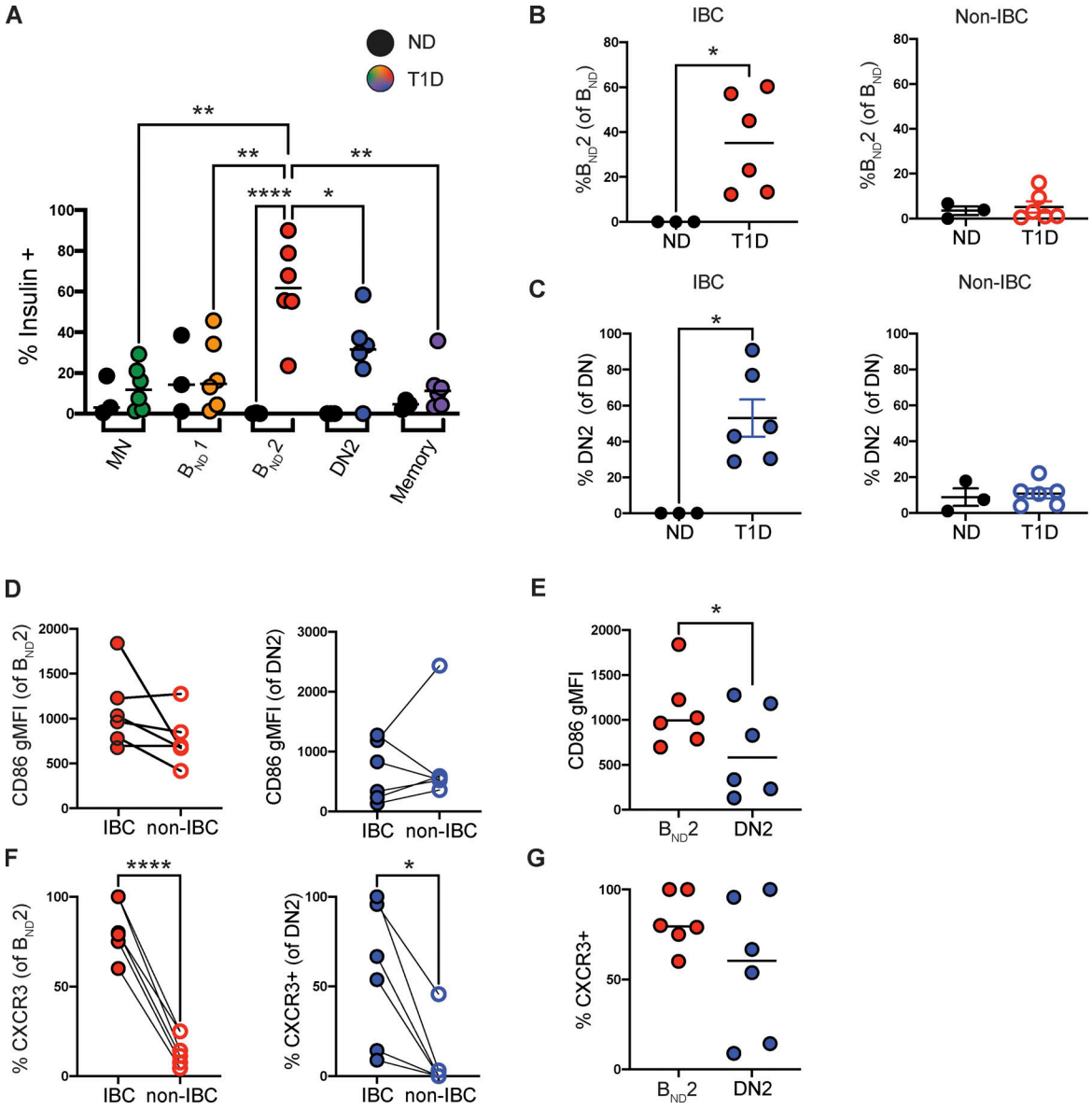

Figure 4. **Insulin-binding $B_{ND}2$ cells are increased in the pLN of T1D donors and express increased CD86 expression compared with DN2 cells. (A)** The percentage of insulin-reactive B cells among each B cell subset. Insulin-binding B cells were enriched from the pLN of T1D (n = 6) and ND (n = 3) donors using magnetic beads and analyzed using flow cytometry. $B_{ND}2$ cells are enriched in insulin-reactive B cells in T1D donors compared with MN, $B_{ND}1$, DN2, and memory (gated as $CD27^+$) B cells. ND control donors have decreased levels of insulin-reactive B cells. Differences were determined using a mixed-effects model. **(B)** The percent of insulin-binding (IBC) $B_{ND}2$ cells is increased in T1D donors compared with ND donors. The percentage of non-IBC $B_{ND}2$ cells is not increased, demonstrating islet-antigen specificity of the finding. Statistical significance determined by unpaired Student's t test. **(C)** Insulin-binding DN2 cells are also increased in T1D donors, but not non-IBC DN2 cells. Statistical significance determined by unpaired Student's t tests. **(D)** IBC $B_{ND}2$ cells exhibit increased expression of the activation molecule CD86 on their cell surface compared to non-IBC $B_{ND}2$ cells in T1D donors. CD86 expression among IBC DN2 cells is decreased in 4/6 T1D donors compared to non-IBC DN2 cells. **(E)** CD86 expression is significantly increased in insulin-binding $B_{ND}2$ cells compared to DN2 cells in T1D donors. **(F)** The percent of IBC $B_{ND}2$ cells that are $CXCR3^+$ is significantly increased compared to non-IBC $B_{ND}2$ cells. Similarly, the percentage of IBC DN2 cells that are $CXCR3^+$ is significantly increased compared to non-IBC DN2 cells. **(G)** The percentage of $CXCR3^+$ insulin-binding $B_{ND}2$ cells is increased, though not significantly, compared to insulin-binding DN2 cells in T1D donors. Statistical significance determined by paired Student's t tests for D–G. *P < 0.05, **P < 0.01, ****P < 0.0001.

phosphorylation of Syk, PLCy2, and Akt compared with MN and $B_{ND}1$ cells, suggesting loss of anergy. Given the increased surface expression of CD69, CD80, and CD86 in $B_{ND}2$ cells, the elevated basal phosphorylation of these proximal signaling molecules likely reflects activation. After stimulation, $B_{ND}2$ cells were able to increase levels of phosphorylated Syk, PLCy2, and Akt comparably to MN B cells, suggesting retained ability to respond to stimulation despite elevated basal phosphorylation levels presumably induced by autoantigen in vivo. Interestingly, DN2 cells appeared hyperresponsive to BCR stimulation compared with $B_{ND}2$ cells. Given that we were stimulating B cells with an anti-human IgG H&L F(ab')2 antibody (which should cross-link

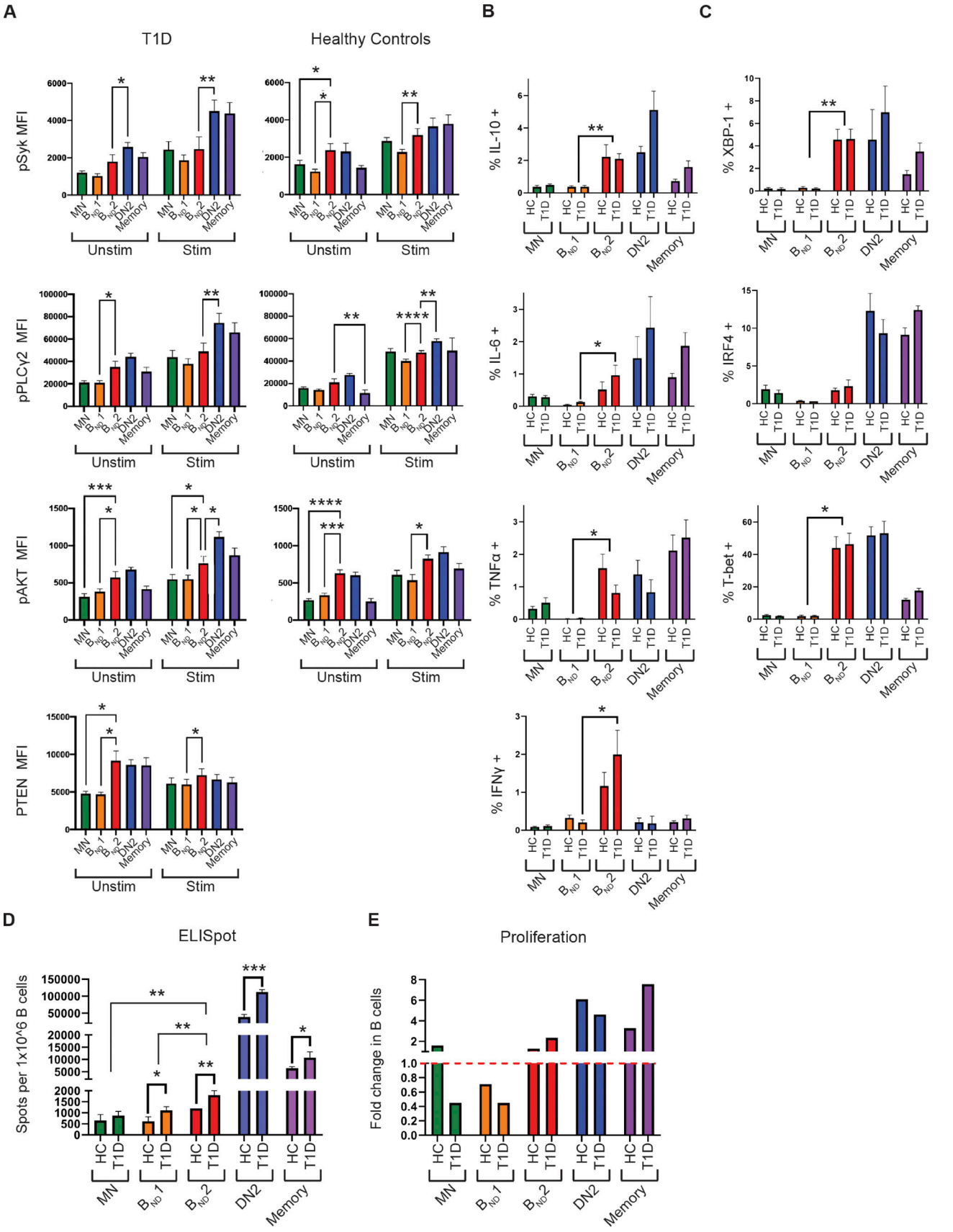

Figure 5. **$B_{ND}2$ cells do not exhibit an anergic B cell phenotype, produce modest amounts of pro-inflammatory cytokines, and display features consistent with pre-ASCs. (A)** $B_{ND}2$ and DN2 cells have higher basal levels of phosphorylated Syk, PLCγ2, AKT compared to $B_{ND}1$ and MN cells, likely

reflecting recent in vivo activation, both in T1D (n = 5) and HC (n = 5) donors. $B_{ND}2$ cells are still able to mount a signaling response similar to MN B cells after stimulation with anti-IgG F(ab′)2 H&L, suggesting they are not anergic. $B_{ND}2$ and DN2 cells have elevated levels of the inhibitory signaling molecule PTEN, which may also reflect recent in vivo activation. **(B)** $B_{ND}2$ cells produce increased levels of IL-10, IL-6, TNF-α, and IFN-γ compared with $B_{ND}1$ cells after 6 h in the presence of a protein transport inhibitor. Cytokine production by $B_{ND}2$ cells is similar to DN2 and memory ($CD27^+$) B cells, with the exception that $B_{ND}2$ cells produce some IFN-γ, but not DN2 cells. **(C)** $B_{ND}2$ and DN2 cells have increased expression of the transcription factor XBP-1, which is associated with plasma cell differentiation. DN2 cells, but not $B_{ND}2$ cells, have increased expression of IRF4, another transcription factor for plasma cell differentiation. $B_{ND}2$ cells have similar levels of the transcription factor T-bet to DN2 cells, which is significantly elevated compared to $B_{ND}1$ cells. **(D)** $B_{ND}2$ cells display increased differentiation into ASCs compared to MN and $B_{ND}1$ cells, but not to the level of DN2 or memory B cells. B cells from T1D donors differentiate into more ASCs compared to HC donors. **(E)** The level of proliferation after in vitro culture for ELISpot assay was determined. $B_{ND}1$ cells undergo cell death, while $B_{ND}2$ cells were maintained or slightly proliferated. Dashed red line represents proliferation (above) or loss of cells (cell death). Data presented are from T1D (n = 5) and HC (n = 5) donors. Statistical significance determined by mixed-effects model. *P < 0.05, **P < 0.01, ***P < 0.001, ****P < 0.0001.

all BCR isotypes by virtue of their light chain) and a larger fraction of DN2 cells have class-switched to IgG, we hypothesize the apparent hyperresponsiveness of DN2 cells is due to enhanced crosslinking of their BCR through both their heavy and light chains (Fig. 5 A). In line with this, comparison of stimulation levels of DN2 cells to $CD27^+$ memory B cells showed similar levels (data not shown).

Next, given previous findings that anergic B_{ND} cells express elevated levels of PTEN, a negative regulator of the PI3-kinase pathway, compared with MN B cells (Smith et al., 2019), we wondered how PTEN levels compared between $B_{ND}1$ and $B_{ND}2$ cells now that we have divided the B_{ND} subset into two populations. We found that $B_{ND}2$, but not $B_{ND}1$ cells, express elevated levels of PTEN compared with MN B cells. In addition, $B_{ND}2$ cells from T1D donors expressed significantly more PTEN than $B_{ND}2$ cells from HC (*P < 0.05; Fig. 5 A; significance not shown). Once again, we hypothesize this likely reflects recent in vivo antigen stimulation and activation. Interestingly, despite the elevated levels of PTEN in $B_{ND}2$ cells from T1D donors, these cells are able to phosphorylate Akt, which is downstream of the PI3-kinase pathway, upon BCR stimulation, suggesting possible impaired inhibitory receptor signaling in T1D subjects. Overall our data suggest that $B_{ND}2$ cells are distinct from $B_{ND}1$ cells, in that they exhibit signs of recent in vivo activation through their BCR, and are able to mount a signaling response after ex vivo BCR stimulation.

$B_{ND}2$ cells produce increased cytokines compared to $B_{ND}1$ cells

Next, we wanted to further evaluate the potential effector function of $B_{ND}2$ cells in the pathogenesis of T1D. B cells have the capacity to act as regulatory cells through production of anti-inflammatory cytokines, e.g., IL-10 and IL-35, as well as effector cells through production of proinflammatory cytokines, e.g., IL-6, TNF-α, and IFN-γ. Therefore, we analyzed the ability of ex vivo $B_{ND}2$ cells to produce various cytokines without stimulation in the presence of a protein transport inhibitor for 6 h. Overall, we found that a small fraction of all B cells produced significant levels of cytokines. Nonetheless, $B_{ND}2$ cells did produce significantly increased levels of IL-10, IL-6, and TNF-α, relative to $B_{ND}1$ cells, while $B_{ND}2$ cytokine production is similar to DN2 and memory ($CD27^+$) B cells. Interestingly, only $B_{ND}2$ cells produced detectable levels of IFN-γ, which are significantly increased in T1D donors (Fig. 5 B). $B_{ND}1$ cells had the lowest cytokine production ability, indicative of their state of anergy. These data suggest that $B_{ND}2$ cells are not a regulatory B cell subset induced in young-onset T1D; rather, these cells could serve as modest producers of proinflammatory cytokines.

$B_{ND}2$ cells express increased levels of the transcription factors XBP-1 and T-box transcription factor (T-bet)

Given that $B_{ND}2$ cells express some markers of plasmablasts, we next wondered whether these cells express increased levels of transcription factors known to promote differentiation into plasmablasts/cells. We found that $B_{ND}2$ cells express significantly increased levels of XBP-1, but not IRF4, compared with $B_{ND}1$ cells. The level of XBP-1 in $B_{ND}2$ cells is similar to DN2 cells. On the other hand, DN2 cells expressed significantly elevated levels of IRF4 compared with $B_{ND}2$ cells (Fig. 5 C). These data suggest that $B_{ND}2$ cells exhibit features consistent with pre-ASCs, but that DN2 cells are likely further along the ASC differentiation path. Given the increased expression of CD11c on $B_{ND}2$ cells, we next compared levels of T-bet, which has been well characterized as upregulated in $CD11c^+$ B cells in both mice and humans (Jenks et al., 2018; Racine et al., 2008; Rubtsov et al., 2011). $B_{ND}2$ cells demonstrate significantly elevated levels of T-bet compared with $B_{ND}1$ cells, and the levels are comparable with that of DN2 cells (Fig. 5 C).

$B_{ND}2$ cells display increased ability to differentiate into ASCs compared to $B_{ND}1$ cells

Next, we wanted to test the ability of $B_{ND}2$ cells to differentiate into ASCs. We used as stimulus a combination of IL-2 and TLR7 agonist R848, which are known inducers of ASC differentiation (Jahnmatz et al., 2013; Pinna et al., 2009), and IL-21, which mimics T follicular helper cell help and was previously shown to be required for the differentiation of DN2 cells into ASCs (Jenks et al., 2018). We found that $B_{ND}2$ cells produce significantly more antibodies than $B_{ND}1$ or MN B cells, but significantly less than DN2 or memory B cells (Fig. 5 D). These data suggest that while $B_{ND}2$ cells are more prone to become ASCs than $B_{ND}1$ cells, they are likely not as far along the ASC differentiation path as DN2 or memory B cells, which is consistent with findings regarding plasma cell transcription factor expression. Interestingly, $B_{ND}1$, $B_{ND}2$, DN2, and memory B cells, but not MN B cells, from T1D donors made significantly more antibody than HC donors, suggesting T1D individuals may be hyperresponsive to IL-21, IL-2, and/or TLR7 stimulation. Previous studies have demonstrated that classic anergic self-reactive B cells have a decreased lifespan compared with non-self-reactive B cells (1–5 d compared with 40 d, respectively; Fulcher and Basten, 1994; Tough and Sprent,

1995). Hence, we wondered whether $B_{ND}2$ cells exhibit a reduced half-life after stimulation with IL-21, IL-2, and R848. We found that while approximately half of all $B_{ND}1$ cells died in culture during this time period, $B_{ND}2$ cells proliferated slightly but not to the same extent as DN2 or memory B cells (Fig. 5 E). This finding suggests that $B_{ND}2$ cells have likely been rescued from anergy-induced cell death through recent activation and receipt of T cell help in vivo.

$B_{ND}2$ and DN2 cells share a transcriptional profile distinct from $B_{ND}1$ cells and consistent with pre-ASC status

To further define the phenotypes of $B_{ND}2$, $B_{ND}1$, and DN2 cells, we compared their transcriptional profiles. We combined single-cell RNA sequencing (scRNA-seq) with CITE-seq (cellular indexing of transcriptomes and epitopes) to enable identification of our $B_{ND}2$ subset among total HC B cells. Clustering analysis identified 11 unique B cell subsets, including naive, activated naive (aN), resting memory, class-switched memory, activated memory, $B_{ND}2$, and DN2 cells (Fig. 6 A). $B_{ND}1$ cells were not initially identified in this clustering analysis. The top 10 differentially expressed genes (DEGs) are shown in Fig. 6 B for each subset identified. Overall $B_{ND}2$ cells exhibit a similar transcriptional profile to DN2 cells. Interestingly $B_{ND}2$ cells appear enriched in the IGHV4-34 gene segment compared with DN2 cells. Previously, it has been demonstrated that the VH4-34 gene segment encodes self-reactive antibodies, and VH4-34 encoded B cells are increased in DN2 cells and SLE patients (Jenks et al., 2018; Richardson et al., 2013). Next, we compared differences in gene expression of various selected genes that are known to be associated with plasma cell differentiation, activation or inhibitory receptors, the DN2 B cell subset, and immunoglobulin isotypes. Overall, we found that $B_{ND}2$ cells share a very similar gene expression profile with DN2 cells, including increased expression of *ITGAX* (CD11c), *TBX21* (T-bet), *FCRL5*, and *HCK*, with the notable exception of *IGHD* and *IGHM*, which were highly expressed in $B_{ND}2$ but not DN2 cells. In addition, $B_{ND}2$ cells have increased expression of genes associated with plasma cell differentiation, including *XBP1*, *IRF4*, and *IL21R*, as well as genes encoding activation molecules, such as *CD80*, *CXCR3*, and *CD1C* (Fig. 6 C). Next, we did a pair-wise comparison of DEGs among DN2 and $B_{ND}2$ cells. While there were only a handful of statistically significant DEGs among these two subsets, we did find that $B_{ND}2$ cells exhibit significantly more expression of genes associated with a naive B cell, such as *IGHM*, *IGHD*, *CD79B*, *FOXP1*, and *FCER2* (CD23), as well as *NIBNA3*, which has been shown to be involved in BCR signaling and B cell apoptosis (Hong et al., 2019; Fig. 6 D). Lastly, given that $B_{ND}1$ cells were not identified as their own unique cluster in our initial analysis, we went back to our CITE-seq data and gated on $B_{ND}1$ and $B_{ND}2$ cells as $CD27^-IgM^{lo}IgD^+CD21^+$ and $CD27^-IgM^{lo}IgD^+CD21^-$, respectively, using CITE-seq antibodies. Analysis of DEGs between these two subsets confirmed that $B_{ND}2$ cells were more similar to DN2 cells than to $B_{ND}1$ cells, in that they have increased expression of *HCK*, *TBX21*, *FCRL5*, and *FGR* compared with $B_{ND}1$ cells. On the other hand, $B_{ND}1$ cells express more *CCR7*, *CXCR4*, and *IL4R*, indicative of a more immature tissue homing phenotype (Fig. 6 E).

CD40-L, IL-21, and TLR7 drive differentiation of $B_{ND}1$ cells into $B_{ND}2$ cells

Finally, we wanted to formally test which conditions provide the best signals for the differentiation of $B_{ND}1$ cells into $B_{ND}2$. Hypothesizing that $B_{ND}1$ cells have already received signal 1 in the form of antigen stimulation through the BCR, we tested various combinations that would provide signal 2 (T cell help) and/or signal 3 (TLR engagement) to sorted $B_{ND}1$ cells. In addition, given that $B_{ND}2$ cells express high levels of T-bet, we also included IFN-γ, which has been shown to induce upregulation of T-bet expression (Lighvani et al., 2001). We found that after 4 d of in vitro stimulation and/or culture, $B_{ND}1$ cells tend to adopt a more MN ($CD27^-IgM^+IgD^+$) phenotype, suggesting loss of anergy (Fig. 7, A and B; and Fig S3). This is likely due to a lack of chronic antigen stimulation once $B_{ND}1$ cells are removed from their in vivo environment in which autoantigen is present (Gauld et al., 2005). The combination of CD40-L, IFN-γ, IL-21, and R848 together provide the best combination of signals to maintain the B_{ND} phenotype (Fig. 7 B). In addition, we found that a combination of IFN-γ, IL-21, and R848 induced the differentiation of $B_{ND}1$ cells into $B_{ND}2$ cells, and when CD40-L was present the differentiation was greater (Fig. 7, A–C; and Fig. S3). These studies indicate that receipt of T cell help (CD40-L, IL-21) and TLR stimulation (R848) are optimal for induction of $B_{ND}1$ cells into $B_{ND}2$ since missing any one of these components resulted in significantly reduced differentiation. It is important to note that in none of our stimulation conditions were DN2 cells generated, demonstrating the specificity of our stimulation conditions to generate $B_{ND}2$ cells, but not DN2 cells.

Discussion

In this study, we identified a unique B cell subset, $B_{ND}2$, that is enriched in autoreactivity, derives from B_{ND} cells, shows evidence of in vivo activation, and is increased in the blood and pLN of young-onset T1D donors. We show that based on phenotypic markers $B_{ND}2$ cells likely have the capacity to act as potent APCs to cognate T cells, as evidenced by increased expression of CD80 and CD86 on their cell surface and retention of HLA-DR expression. In addition, $B_{ND}2$ cells produce proinflammatory cytokines, which may contribute to the local inflammatory environment in vivo. Importantly, $B_{ND}2$ cells resemble pre-ASCs phenotypically, transcriptionally, and functionally, and frequency of insulin-binding $B_{ND}2$ cells strongly correlates with anti-insulin antibody titers in T1D subjects. Given that young-onset T1D is characterized as fast progressing and aggressive due to more rapid loss of beta cell function compared with older-onset T1D, our findings highlight various potential functions of pathogenic B cells in the young-onset endotype.

Unlike other autoimmune disorders, such as SLE and RA, in which it is well accepted that production of autoantibodies contributes to the pathogenesis of disease, autoantibodies have historically been used to confirm a diagnosis of T1D and predict individuals who are at increased risk of T1D but are not generally considered pathogenic in T1D. Autoantibodies can play a pathogenic role through FcγR-mediated antigen–antibody uptake and activation by dendritic cells and macrophages that then

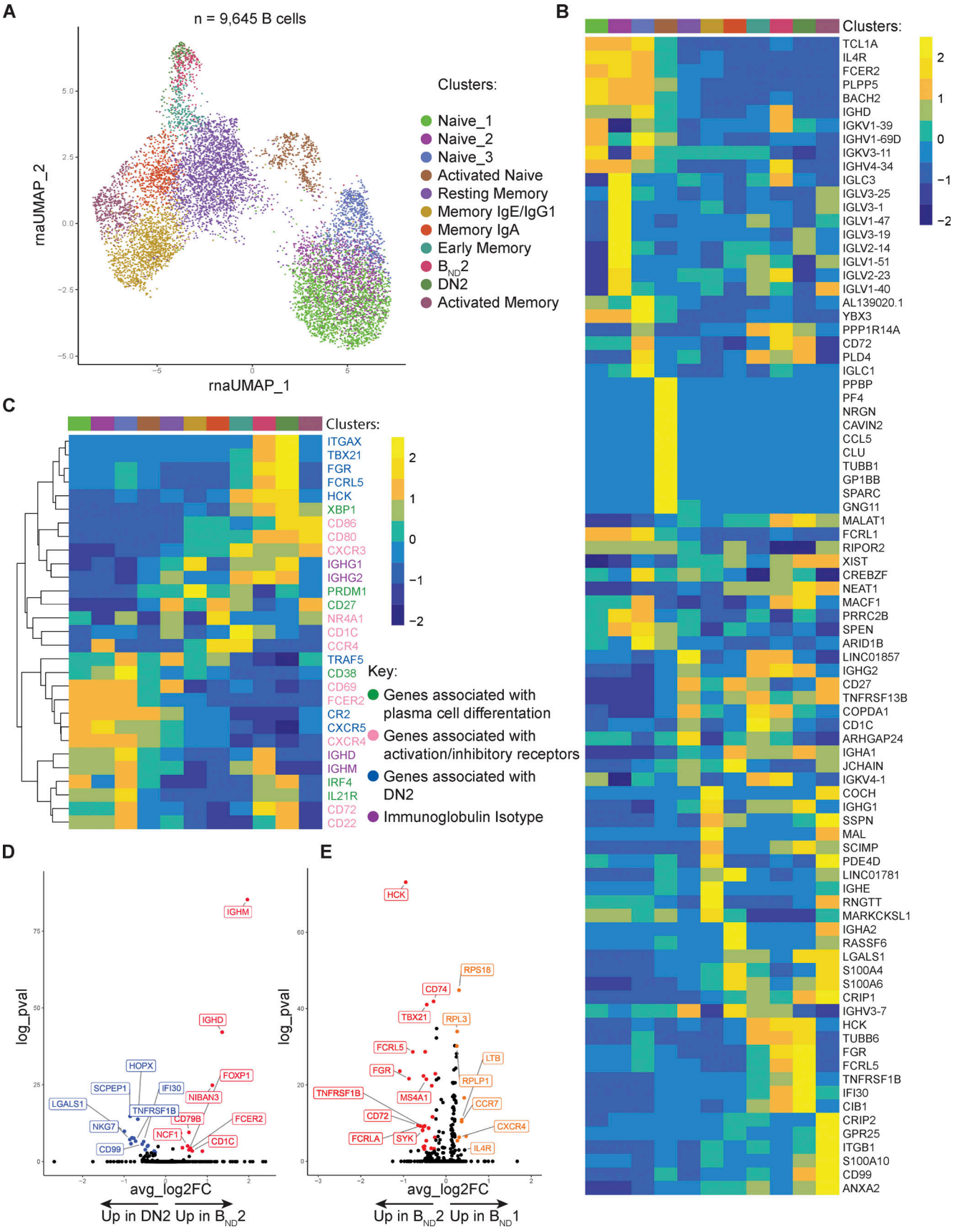

Figure 6. **sc-RNA-seq reveals $B_{ND}2$ and DN2 cells share a similar transcriptome, consistent with pre-ASCs. (A)** UMAP of B cell clusters identified using scRNA-seq. Naming of B cell clusters was based on varying levels of gene expression of markers associated with activation, naive B cells, memory B cells, and/

or isotype. **(B)** Heatmap of top 10 DEGs for each B cell cluster identified in A. **(C)** Heatmap of handpicked genes of interest that are known to be associated with plasma cell differentiation, activation or inhibitory receptors, the DN2 B cell subset, and immunoglobulin isotype. Transcriptionally, $B_{ND}2$ cells are similar to the DN2 subset. **(D)** Volcano plot of DEGs that are significantly different between DN2 and $B_{ND}2$ cells. Blue dots indicate genes that are increased in DN2 cells, while red dots indicated genes that are increased in $B_{ND}2$ cells. Labels for a few hand-picked genes are included. **(E)** Volcano plot of DEGs that are significantly different between $B_{ND}1$ and $B_{ND}2$ cells. Red dots are genes increased in $B_{ND}2$ cells, while dark yellow dots are genes that are increased in $B_{ND}1$ cells. Data are from an HC donor.

present antigen to self-reactive T cells. Inoue et al. demonstrated that FcγR-deficient non-obese diabetic mice were protected from diabetes and insulitis was alleviated (Inoue et al., 2007). Moreover, Silva et al. demonstrated that secretion of anti-islet autoantibodies acts in an FcγR-mediated fashion to enhance the expansion of islet-reactive CD4 T cells in mice (Silva et al., 2011). Furthermore, studies in humans indicate a tight correlation between the number of autoantibody specificities one develops and progression to diabetes. Importantly for this study, of all the possible autoantibodies one can generate during the course of T1D, such as those targeting insulin, GAD65, and IA-2, it has only been shown for anti-insulin antibodies that titer levels correlate with disease progression (Steck et al., 2016; Steck et al., 2011), suggesting a more pathogenic role for anti-insulin antibodies in T1D. Hence, our findings that an increased frequency of insulin-binding $B_{ND}2$ cells, which are pre-ASCs, occurs specifically in young-onset T1D subjects, correlates with anti-insulin antibody titers, and identifies a likely B cell subset responsible for generation of anti-insulin antibodies. Overall, these findings suggest that the pathogenic function of autoreactive B cells in young-onset T1D could include presentation of autoantigen to T cells, production of autoantibodies, and production of proinflammatory cytokines.

$B_{ND}2$ cells share a similar but distinct phenotype with the previously described DN2 B cell subset, in that they both are $CD27^-$ $CD21^-$ $CXCR5^-$, yet $B_{ND}2$ cells express IgD, CD72, CD22, HLA-DR, and CD38 on their cell surfaces. Transcriptionally and functionally $B_{ND}2$ and DN2 are similar. While we cannot exclude the possibility that $B_{ND}2$ cells are precursors to DN2 cells, it is notable that in this study insulin reactivity was restricted to the $B_{ND}1$ and $B_{ND}2$ subsets, which comprise the previously defined autoreactive anergic B_{ND} subset in the peripheral blood, while the amount of insulin-reactive B cells within the DN2 subset was similar to MN B cells. Furthermore, our differentiation studies demonstrate that $B_{ND}1$ cells can be induced to differentiate into $B_{ND}2$ cells, but not DN2 cells, using a combination of CD40-L, IL-21, and R848. It is conceivable that stimulating $B_{ND}1$ cells for a longer period of time or adding or removing other cytokines or soluble factors would enable ultimate differentiation of $B_{ND}1$ cells into DN2 cells. Future studies aim to address this possibility. Taken together, studies reported here indicate that $B_{ND}2$ and DN2 cells are either (1) distinct subsets that arise independently from each other yet share similar phenotypes or (2) $B_{ND}2$ cells are precursors to DN2 cells. However, this would require that another B cell subset, other than $B_{ND}2$ cells, feeds into the DN2 subset or another peripheral tolerance mechanism is in place to decrease the overall level of insulin-reactive B cells in the DN2 subset. Nonetheless, in the present study, frequency of insulin-binding $B_{ND}2$ cells, but not DN2 cells, was found to correlate with disease activity and therefore could serve as therapeutic target in young-onset individuals and/or a biomarker for aggressive disease.

Our $B_{ND}2$ subset also resembles the previously reported aN subset, previously shown to be precursors to DN2 cells and enriched in SLE patients (Jenks et al., 2018; Tipton et al., 2015). One phenotypic difference between $B_{ND}2$ cells and aN cells is that $B_{ND}2$ cells express higher levels of CD38 compared with resting MN B cells, while aN cells lack CD38 expression. In addition, Tipton et al. argue that aN cells arise from resting naive B cells. However, given the enrichment of autoreactivity in $B_{ND}2$ cells and our findings that $B_{ND}1$ cells give rise to $B_{ND}2$ cells in vitro, we believe $B_{ND}2$ cells arise from the anergic B_{ND} subset, which has previously been shown to be enriched in autoreactive clones compared to resting naive B cells. We believe this is a very important distinction between our $B_{ND}2$ cell subset and aN cells.

By combining high dimensional mass cytometry, a B cell–focused antibody panel, antigen specificity, comparison of peripheral blood to the pLN, and functional and transcriptional analyses, this study represents the most in-depth study of the role of B cells in T1D to date. In addition, the findings herein help clarify some of the conflicting reports seeking to identify the diabetogenic B cell in T1D through use of a comprehensive B cell antibody panel, stratification of subjects based on age of onset (i.e., endotype), and the ability to study total B cells, as well as antigen-specific B cells simultaneously. While this study helps answer some questions, it also brings to bear new issues. For example, it remains to be known why only one subset of insulin-reactive B_{ND} cells become activated in T1D and not the rest, even though $B_{ND}1$ and $B_{ND}2$ cells express similar levels of insulin-reactivity in the peripheral blood. Possible non-mutually exclusive explanations include: $B_{ND}2$ cells have impaired inhibitory signaling, higher affinity and more specific BCRs, and/or presented antigen to diabetogenic insulin-reactive T cells that cause disease. B_{ND} cells have been shown to be increased in polyreactivity (Duty et al., 2009; Smith et al., 2015). It remains unknown whether $B_{ND}2$ cells exhibit the same level of polyreactivity as $B_{ND}1$ cells or are more specific. Future studies aim to address this possibility by performing an in-depth analysis of the $B_{ND}2$ cell repertoire, level of somatic mutations, affinity for insulin, and level of polyreactivity compared to $B_{ND}1$ and DN2 cells. In addition, the strong association of the high-risk HLA DR4-DQ8 allele with increased frequency of insulin-reactive $B_{ND}2$ cells, and observations that $B_{ND}1$ cells can be driven to differentiate into $B_{ND}2$ cells by CD40-L and IL-21, implicate receipt of T cell help with breaking anergy and inducing a $B_{ND}2$ cell phenotype.

One limitation of this study was that we did not validate that our enrichment for insulin-binding B cells yields true insulin-

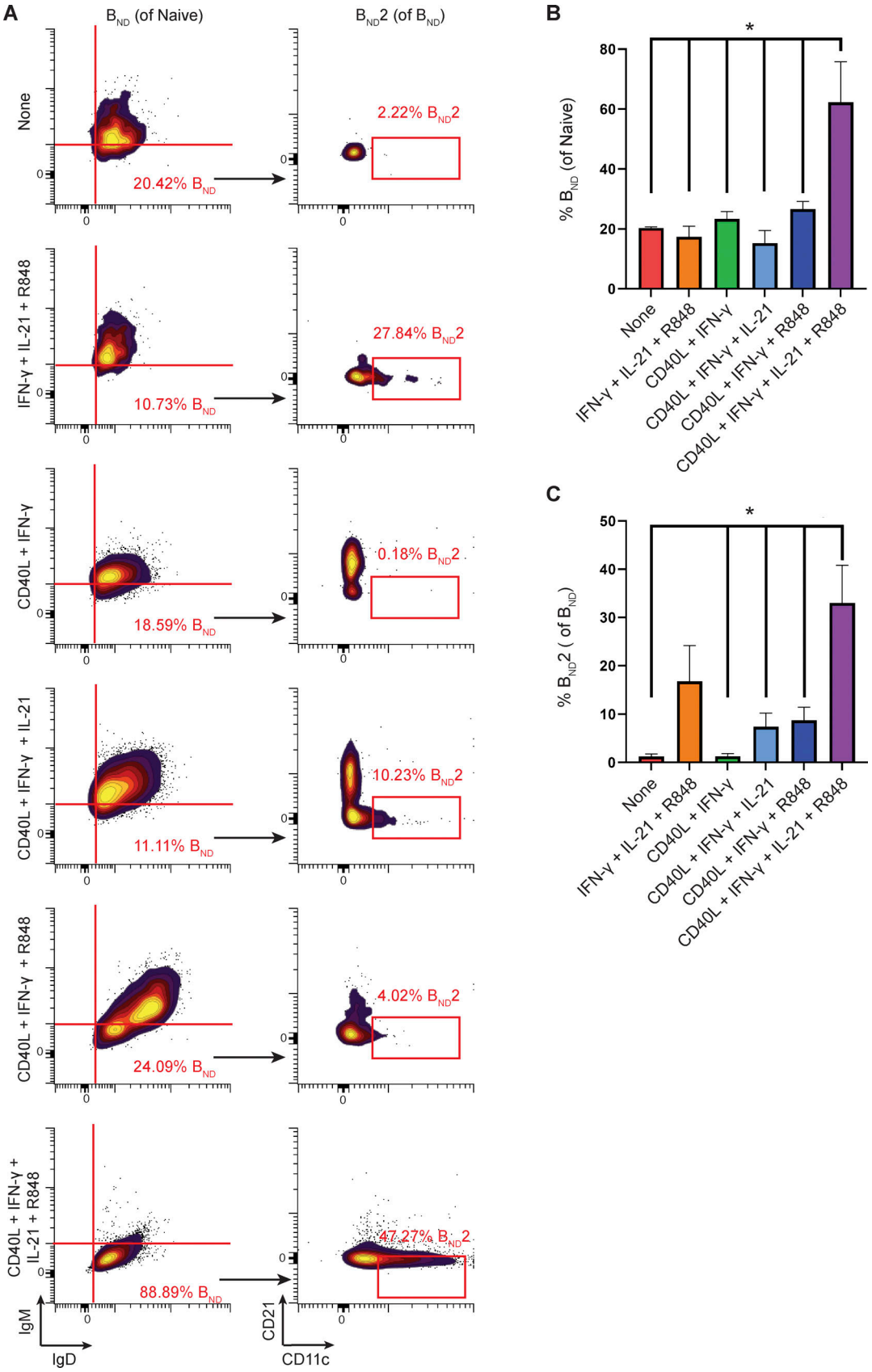

Figure 7. **Differentiation of $B_{ND}1$ cells into $B_{ND}2$ cells is driven by a combination of CD40L, IFN-γ, IL-21, and R848. (A)** Example cytograms of the gating strategy used to identify the percent of retained B_{ND} cells and the percent that differentiated into $B_{ND}2$ cells after stimulation with varying reagents for 4 d. $B_{ND}1$ cells were sorted from HC PBMC samples (n = 4) and stimulated with a combination of different reagents. **(B)** The frequency of $B_{ND}1$ cells that retained a

B_{ND} phenotype ($CD27^-$, IgM^{lo}, IgD^+) after stimulation. **(C)** The frequency of $B_{ND}1$ cells that differentiated into $B_{ND}2$ cells after stimulation. $B_{ND}2$ cells were defined as $CD19^+$ $CD27^-$ IgM^{lo}, IgD^+, $CD21^-$, $CD11c^+$. Overall, using a combination of CD40L, IFN, IL-21, and R848 maintained the B_{ND} phenotype the best, and induced the most differentiation into $B_{ND}2$ cells after stimulation. Data presented are from HC (n = 3) donors, and samples were treated in triplicates. Statistical significance determined by mixed-effects model. *P < 0.05.

reactive B cells. However, previously we have verified that our enrichment strategy does, in fact, isolate insulin-reactive B cells by generating recombinant antibodies with cloned immunoglobulin genes from single-sorted human insulin-binding B cells (Smith et al., 2015). We have also verified our enrichment strategy using anti-insulin BCR transgenic mice compared with other non-insulin BCR reactive transgenic mice, such as the anti-HEL MD4 and Ars/A1 mouse models (Smith et al., 2018a). Hence, in this study, we did not feel that we needed to revalidate that our enrichment procedure is specific. Other limitations of these studies include the relatively low number of T1D and HC subjects per age group in the mass cytometry studies, the relatively low number of T1D and ND pLN samples analyzed, and the lack of age-matched ND pLN samples. While all three ND pLN samples carried the high-risk HLA DR4-DQ8 risk allele, which is an important comparison, future studies are aimed at acquiring young ND pLN samples for proper age-matched control comparisons. In conclusion, this study shows that activation of insulin-reactive anergic B cells and their potential to act as ASCs and APCs likely plays a role in the rapid progression of T1D seen in young-onset T1D subjects and identifies a possible age-appropriate therapeutic target.

Materials and methods

Study participants

All participants were enrolled under study protocols approved by the Colorado Multiple Institutional Review Board (#01–384). Written informed consent was obtained from each adult participant, or from parents or guardians of participants <18 yr old. Assent was obtained from participants over the age of 7 yr who were cognitively able to consent. All procedures were performed in accordance with Colorado Multiple Institutional Review Board guidelines and regulations. Demographics and other data about research participants can be found in Tables 1 and S2.

Samples were obtained with informed consent at the Barbara Davis Center at the University of Colorado Anschutz Medical Campus. Eligible subjects were male or female who had been recently diagnosed (<100 d) with T1D and age-/sex-matched HCs. HLA haplotypes and autoantibody levels against insulin, IA-2, GAD65, ZnT8, TGIgA, and HyD21 were conducted at the Clinical Laboratory Improvement Amendments–certified Autoantibody/HLA Service Center at the Barbara Davis Center for Diabetes. Inclusion criteria for the HC group included (1) autoantibody negative, (2) no history of autoimmune disease, and (3) no history of illness within the last 2 wk. Of our HC group, ∼45% (18/40) were FDRs. No difference in frequency of $B_{ND}2$ cells or DN2 cells was found among FDRs and non-FDRs, and therefore we included both groups in our HC group. Demographics and clinical data of research participants can be found in Tables 1 and S2.

Blood sample processing

Approximately 30 ml of whole blood was collected via venipuncture into sodium heparin vacutainers. Peripheral blood mononuclear cells (PBMCs) were isolated via Ficoll density centrifugation. DNA for HLA typing was extracted from granulocytes using the DNA midi kit (Qiagen). PBMCs for CyTOF analysis, ELISpot, and differentiation assays were processed directly ex vivo. Remaining assays utilized frozen PBMCs from individuals with recent onset T1D and healthy controls.

Mass cytometry sample preparation

Samples were prepared for CyTOF using a previously described method (Stensland and Smith, 2021). Briefly, PBMCs were incubated with 30 µl Fc Block (Miltenyi) for 5 min on ice followed by 0.3 µg/10^6 cells of biotinylated insulin (INS30G100; Eagle Biosciences) and 0.25 µg/10^6 cells of FITC labeled tetanus toxoid (Colorado Serum Company). Insulin-binding and tetanus-binding B cells were enriched using the recommended amount of cleavable anti-biotin and anti-FITC magnetic beads (Miltenyi). Postenrichment, magnetic beads were cleaved, depleted fractions were stained with CD45-89Y, and enriched fractions were stained with CD45-113Cd. These fractions were then washed, combined, and stained with an antibody mastermix (Table S2) for B cell–specific surface markers, as well as metal-labeled anti-biotin and anti-FITC to identify insulin-binding and tetanus-binding B cells, respectively. Individual samples were intercalated for a minimum of 48 h before being run on the Helios mass cytometer.

Mass cytometry analysis

Preprocessing for algorithm-based analysis

Files were instrument/bead normalized and debarcoded using Matlab Normalizer and Debarcoder Tool. Preprocessing of individual FCS files was done in R using CytoTree to identify and isolate live B cells ($CD45^+CD3^-CD19^+$). Batch effects were corrected in CytoTree. Enriched and depleted fractions were separated by their respective CD45 antibody signals into individual files. While both enriched and depleted fractions were used in analysis, only enriched fractions were used in dimensional reduction and clustering analysis. To ensure equal representation, individual files were downsampled to 1,000 events and given unique identifiers before being concatenated into a CYT object normalized to Arcsinh.

Algorithm-based analysis

Uniform Manifold Approximation and Projection (UMAP) was chosen as the method for dimensional reduction (Metric: Euclidean, Neighbors: 15, minimum distance: 0.5) while PhenoGraph and Self-organizing map methods were used for clustering (K = 15, xdim = 8, ydim = 6) using the following markers: CD22, CD5, CD69, CD95, IgD, CD20, CD38, CD24, CD86,

CD36, CD40, CD27, CXCR3, CD10, CD80, CD11c, CD72, CD71, CXCR5, CD23, CD138, IgG, PD-L1, IgM, CD21, CCR4, and PD-1. The xdim and ydim values were determined based on the number of clusters that could be generated with high resolution (n = 48) while decreasing the workload and user bias when identifying and merging clusters deemed phenotypically too similar to be considered a separate population. Clusters were defined using phenotypic heatmap data (e.g., cluster 10 was identified as CD27$^+$ IgG$^+$ CD38$^{lo/+}$, and therefore, labeled "IgG memory"), a priori knowledge of established B cell subsets, and comparison of UMAP defined clusters to manual gating clusters. Clusters that were found to share very similar phenotypes and could not be distinguished through manual gating were merged together. Populations of interest were validated through manual gating in FlowJo and Cell Engine where these gating strategies were used to compare population frequencies and marker expression between individuals and disease state groups. For Fig. 1, unbiased UMAP projections were run on HC and T1D donors separately. Insulin$^+$ and tetanus$^+$ gates were determined using a combination of (1) analysis of CD3$^+$ T cells that are both negative for insulin and tetanus to determine the cutoff of negative versus positive and (2) analysis of depleted cell fractions (unenriched) to determine the cutoff for negative versus positive gates.

nPOD donor sample processing and preparation

pLN samples were cut and dissociated through a 70-µM cell strainer to obtain a single-cell solution. Cells were incubated with the following surface marker antibodies: anti-CD71-BUV395, anti-CD27-BUV563, anti-CD86-BV421, anti-CD19-BV510, anti-IgM-BV650, anti-CXCR3-BV711, anti-CD24-Bv785, anti-IgD-FITC, anti-CD3-PerCP, anti-CXCR5-PE/Dazzle510, anti-CD21-PECy7, and anti-CD38-APCFire810 (all BioLegend) and 0.3 µg/10^6 cells of biotinylated insulin (Eagle Biosciences) for 15 min on ice. Cells were then washed twice and fixed in 2% paraformaldehyde (PFA) for 5 min. Cells were washed and then incubated with anti-biotin magnetic microbeads (Miltenyi) per manufacturer's instructions. Insulin-binding B cells were enriched using MACS LS columns. Enriched and depleted fractions were incubated with 1:2,000 Steptavidin-AF647 (BioLegend) for 10 min on ice. Cells were washed twice and fixed in 2% PFA in preparation for flow cytometry.

Phosflow assays

Frozen PBMCs from individuals with T1D and HCs were thawed and resuspended in prewarmed serum-free RPMI at 10^7 cells/ml and allowed to sit for 30 min at 37°C to return to basal phosphorylation levels. Samples were then resuspended in prewarmed 5% FBS RPMI at 10^7 cells/ml. Samples were divided into triplicate samples and either received a stimulation mastermix containing both surface antibodies (anti-CD19-BV510, anti-CD27-BUV563, anti-IgM-BV650, anti-IgD-FITC, and anti-CD11c-APC-Cy7 [all BioLegend]) and 10 µg/ml anti-human IgG (H&L) F(ab′)2 (Jackson Immunoresearch) or a mastermix of only surface antibodies and allowed to stain/stim for 5 min at 37°C before being fixed with 2% PFA. Cells were then permeabilized with 500 µl of BD Cytofix/Perm for 30 min, washed twice with BD Perm/Wash buffer, and then stained with anti-pSyk-PE/Cy7 (BD), anti-pPLCy2-PE (BD), anti-pAKT-AF647 (BD), PTEN-BV421 (BD), or isotype control mastermix for 45 min on ice. Cells were washed twice with BD Perm/Wash buffer and then fixed in 2% PFA in preparation for flow cytometry.

Intracellular cytokine assays

Frozen cells from individuals with T1D and HCs were used and divided into six equal samples. Triplicate samples were analyzed at baseline (T0) with no exogenous stimulation or after 6 h (T6) in the presence of the protein transport inhibitor, Brefeldin-A (BioLegend) at 1× for 37°C. T0 and T6 samples were stained with the surface antibody mastermix (anti-CD19-BV510, anti-CD27-BUV563, anti-IgM-BV650, anti-IgD-FITC, anti-CD11c-APC-Cy7 [all BioLegend]), fixed with 2% PFA, and then permeabilized in 500 µl BD Cytofix/Perm. Samples were then either stained with an intracellular antibody mastermix (anti-IL-10-BV421, anti-TNF-α-Alexa647, and anti-IFN-γ-PE or anti-IL-6-PE [all BioLegend]) or corresponding isotype control mastermix at 4°C for 45 min. Cells were washed twice with BD Perm/Wash buffer and then fixed in 2% PFA in preparation for flow cytometry. To serve as a positive control for cytokine antibody staining and gating for flow cytometry, a healthy control sample was stimulated in triplicate with 1× Cell Activation Cocktail with Brefeldin-A (BioLegend) for 6 h at 37°C and stained and processed as above.

Transcription factor assays

Frozen cells from individuals with T1D and HCs were thawed and stained in triplicate with a surface antibody mastermix (anti-CD27-BUV563, anti-CD19-BV510, anti-IgM-BV650, anti-IgD-FITC, and anti-CD11c-APC-Cy7 [all BioLegend]) for 15 min on ice, washed twice, and then permeabilized with BD Cytofix/Perm for 30 min on ice. Cells were then stained either with an intracellular mastermix (anti-IRF4-PE, anti-XBP1-AF647, anti-T-bet-PE/Cy7 [all BioLegend]) or corresponding isotype control mastermix at 4°C for 45 min. Cells were washed twice with BD Perm/Wash buffer and then fixed in 2% PFA in preparation for flow cytometry.

Cell sorting for ELISpot and differentiation assays

Fresh PBMCs were enriched for B cells using Miltenyi No Touch B cell enrichment kit. B cells were then stained with a surface antibody mastermix (anti-CD19-BV421, anti-IgM-BV650, anti-IgD-FITC, anti-CD11c-PE, and anti-CD27-PE-Cy7) for 15 min on ice and washed twice with FACS buffer. For ELISpot assays, B cells were then sorted on the Astrios Cell Sorter (Beckman Coulter) into memory B cells (CD27$^+$), MN B cells (CD27$^-$, IgM^{hi}, IgD$^+$), $B_{ND}1$ (CD27$^-$, IgM^{lo}, IgD$^+$, CD11c$^-$), $B_{ND}2$ (CD27$^-$, IgM^{lo}, IgD$^+$, CD11c$^+$), and DN2 (CD27$^-$, IgM$^-$, IgD$^-$, CD11c$^+$) fractions. For B cell differentiation assays, $B_{ND}1$ cells were only sorted.

ELISpot assays

Sorted B cell populations were stimulated with 50 ng/ml IL-21 (BioLegend), 1 µg/ml R848 (Invivogen), and 50 ng/ml IL-2 (BioLegend) in 10% FCS RPMI for 5 d at 37°C. ELISpot plates were coated with 100 µl of 5 µg/ml goat anti-human IgG (H&L; Southern Biotech) per well overnight before being blocked with 10% FCS RPMI for 2 h the following day. After 5 d, cells from

each subset were recounted, resuspended, plated, and serial diluted onto the blocked precoated ELISpot plate before being allowed to incubate overnight at 37°C. The following day, cells were washed removed with 0.05% Tween in PBS and lysed with 100 µl cold MilliQ water. Then 100 µl of 1:2,000 diluted goat anti-human IgG (H&L)-AP (Southern Biotech) was added to each well and allowed to incubate at room temp for 3 h before being washed with 0.05% Tween in PBS. 100 µl of 5-bromo-4-chloro-3-indolyl phosphate buffer (Thermo Fisher Scientific) was added to each well and allowed to incubate until spots formed. Plates were then washed with double distilled water and allowed to dry overnight before being analyzed on a CTL plate reader.

$B_{ND}1$ cell differentiation assays

Sorted $B_{ND}1$ cells were stimulated for 4–5 d in 10% FCS + RPMI with varying combinations of the following stimulation reagents: IFN-γ (20 ng/ml), CD40-L (2 µg/ml), R848 (1 µg/ml), and/or IL-21 (50 ng/ml). Cells were then stained with a surface antibody mastermix (anti-CD19-BV421, anti-IgM-BV650, anti-CXCR3-BV711, anti-IgD-FITC, anti-CD11c-PE, anti-CXCR5-PE/Dazzle594, anti-CD27-PE-Cy7, anti-CD21-APC, and anti-CD38-APC-Fire810 [all BioLegend]) for 15 min on ice. After staining, cells were washed twice with FACS buffer and then fixed in 2% PFA in preparation for flow cytometry.

scRNA-seq

B cells from fresh PBMCs were isolated using the Miltenyi No Touch B cell Enrichment Kit. Cells were then divided in half, one for scRNA-seq and one for flow verification/comparison. Samples for scRNA-seq were stained with Total-Seq antibodies (BioLegend) at 1 µg/10^6 cells for the following surface markers: IgD, IgM, CD27, CXCR5, and CD21 for 20 min on ice, washed twice with FACS buffer, and then resuspended in 1× PBS. Cells were then prepared for scRNA-seq using the 10X Genomics platform per the manufacturer's instructions (see below). For the flow cytometry parallel samples, B cells were stained with antibodies of the same clone as Total-Seq antibodies using the following panel: anti-CD27-BUV563, anti-CD19-BV510, anti-IgM-BV650, anti-IgD-FITC, anti-CXCR5-PE/Dazzle594, and anti-CD21-PE/Cy7 (all BioLegend) for 15 min on ice, washed twice with FACS buffer, and then fixed in 2% PFA in preparation for flow cytometry.

scRNA-seq preparation

A single-cell suspension of B cells previously stained with Total-Seq antibodies was prepared at 1,000 cells/µl for capture of 10,000 cells on the Chromium Next GEM Chip G for 5′ capture gel beads. Following single-cell capture and GEM-RT Cleanup, as described in the Chromium Next GEM Single Cell V(D)J Reagent Kits v1.1 User Guide Rev F, a cDNA amplification reaction was prepared with the addition of an appropriate primer to amplify the Total-Seq antibody oligo (feature barcode) sequences in addition to captured mRNA. After cDNA amplification, the supernatant from the 0.6× SPRIselect size selection was saved and used downstream for analysis of the feature barcodes contained in that smaller size fraction. The 5′ Gene Expression Library Construction was done as described in the previously mentioned User Guide for the mRNA Gene Expression Library. For the Feature Barcode (ADT) Library preparation, the CITE-seq protocol from the New York Genome Center Technology Innovation Lab Version: 2019-02-13 was followed using the retained supernatant from the cDNA cleanup. Unique indexes were added to the 3′ and 5′ ends of the ADT library molecules with 2× PCR NEB High Fidelity with Q5 Polymerase Master Mix for downstream demultiplexing and data analysis.

Sequencing data analysis

Preprocessing

Sequences from scRNA-seq and scCITE-seq were processed using 10X Genomics Cellranger v6.0.1 software (Zheng et al., 2017) with the cellranger GRCh38-2020-A genome and gtf file. Raw data generated by Cellranger were then read into R (v4.1.2) using the Seurat (Hao et al., 2021) v4.1.0 R package with at least 200 genes per cell and at least three cells. Cells were further filtered based on the number of genes per cell (between 500 and 4,000), the number of ADT reads (<2,000), and the percent of mitochondrial reads per cell (<10%). After filtering, 10,737 were used for downstream analysis. The data were normalized by using "NormalizeData." For each sample, variable genes were found by using "FindVariableFeatures" and data were scaled using "ScaleData." Doublets were removed using "DoubletFinder" (McGinnis et al., 2019) using the default values except for pK, nExp, and PCs (pk = 0.14, nExp 32, PCs = 1:10). After doublet removal, 9,910 cells were used for downstream analysis. CITE-seq antibodies were normalized using "DSBNormalizeProtein" from the dsb package (v0.3.0; Mulè et al., 2022).

Dimensionality reduction and clustering

Dimensionality reduction and clustering were performed using "RunPCA," "FindNeighbors," "FindClusters," and "RunUMAP." "RunPCA" was run using the default values except all variable features were used for the features argument. "FindNeighbors" was run with default parameters except for the dims argument (dims = 1:14). "FindClusters" was run with default parameters except for the resolution argument (resolution = 0.8). "RunUMAP" was run with default parameters except for the dims and metric arguments (dims = 1:14, metric = "correlation").

Cell type identification

We made a first pass at naming clusters using a bulk RNA high-quality dataset (Calderon et al., 2019) as a reference and determining cluster identity using "clustifyr" (Fu et al., 2020). To generate the reference, we downloaded the RNA_gene_abundance file from GEO accession no. GSE118165 and mapped the Ensembl IDs to gene IDs. We then used this matrix as in "clustify" from "clustifyr" as the "ref_mat" argument. We used the top 2,000 variable genes as the "query_genes" and the clusters identified by "FindClusters" as the "cluster_col" The top correlated cell type to each cluster was used as the first determination of cell type.

Subsetting, dimensionality reduction, and clustering

After naming cell types, we found a small number of T cells (195), monocytes (23), and undetermined cells (27). We removed

these cells and only kept cells identified as B cells (9,665). Following subsetting, we repeated finding variable genes and scaling the data ("FindVariableFeatures" and "ScaleData"). We repeated dimensionality reduction and clustering on the subset of cells. "RunPCA" was run using the default values except all variable features were used for the features argument. "FindNeighbors" was run with default parameters except for the dims argument (dims = 1:14). "FindClusters" was run with default parameters except for the resolution argument (resolution = 0.6). "RunUMAP" was run with default parameters except for the dims and metric arguments (dims = 1:14, metric = "correlation"). To identify markers of each cluster, "FindAllMarkers" was run using default settings except we set only.pos to TRUE. Genes were called differentially expressed if the adjusted P value was <0.05 and the log-fold change was >0.5. To generate a heatmap of markers, the average expression of all genes within each cluster was determined using "AverageExpression" from Seurat. Next, the top 10 markers based on log fold change were selected for each cluster and the average expression matrix was subset to only those genes. Finally, a z-score was computed and the plot was generated with "pheatmap" (https://cran.r-project.org/web/packages/pheatmap/index.html).

Cluster 6 subsetting and reclustering

To locate the clustering that contained the $B_{ND}2$ cells, we used our CITE-seq antibodies to locate cells that were IgD positive (the top 50% of IgD expression), IgM low (the bottom 95% of IgM expression), and CD21 negative (bottom 10% of cells). Many of the cells matching these cutoffs were in cluster 6 (10% of total cells in the cluster). To gain better resolution of this cluster, we subset the data to only cluster 6 and reprocessed. Following subsetting, we repeated finding variable genes and scaling the data ("FindVariableFeatures" and "ScaleData"). We repeated dimensionality reduction and clustering on the subset of cells. "RunPCA" was run using the default values except all variable features were used for the features argument. "FindNeighbors" was run with default parameters except for the dims argument (dims = 1:7). "FindClusters" was run with default parameters except for the resolution argument (resolution = 0.4). "RunUMAP" was run with default parameters except for the dims and metric arguments (dims = 1:7, metric = "correlation"). Three clusters were identified by this analysis (early memory, $B_{ND}2$, and DN2). We added these three clusters to the full dataset in place of cluster 6.

B cell subset comparisons

To compare the DN2 and $B_{ND}2$ populations, we also used the "FindMarkers" function from Seurat and kept genes with an adjusted P value less than 0.05. To compare $B_{ND}1$ to $B_{ND}2$ cells, $B_{ND}2$ cells were found as described above (IgD positive, IgM low, and CD21 negative). $B_{ND}1$ cells were similarly identified but were IgD positive, IgM^{lo}, and CD21 positive (top 25% of cells). We performed differential expression between these two populations using the "FindMarkers" function from Seurat and kept genes with an adjusted P value less than 0.05. All scripts to replicate this analysis are on github (https://github.com/CUAnschutzBDC/Smith_210825_b_cell_analysis).

Mass and flow cytometry analysis

Analysis of mass and flow cytometry samples was done either in FlowJo (Treestar) or Cell Engine. Files that required recompensation were compensated in FlowJo.

Statistical analysis

Data were analyzed using Prism software (GraphPad Software, Inc.). Differences between B cell subsets (Fig. 2, Fig. 4 A, and Fig. 5) were analyzed using a mixed-effects model or paired Student's *t* test (Fig. 4, D–G). Differences between T1D and controls were analyzed using one-way ANOVA with Tukey multiple comparisons post-test. Correlations were determined using Spearman correlation. A P value of ≤0.05 was considered statistically significant and is denoted by an asterisk, in which * ≤ 0.05, ** ≤ 0.01, and *** ≤ 0.001. All error bars are shown as mean ± SEM.

Online supplemental material

Table S1 lists all antibodies used in the mass cytometry B cell panel. Table S2 includes all patient demographics and available clinical data, such as HLA haplotype and autoantibody titers. Fig. S1 displays heat maps of surface marker expression levels in the B cell subsets identified by unsupervised clustering for T1D and HC donors. Fig. S2 are UMAP projections of insulin-binding, tetanus-binding, and non-binding B cells from T1D and HC donors. Fig. S3 presents cytograms of the B cell phenotype of BND1 cells after stimulation with various combinations of reagents in vitro after 5 d.

Data availability

The data underlying Figs. 1, 2, 3, 4, 5, and 7 are available from the corresponding author upon reasonable request. The data underlying Fig. 6 are openly available on GEO with accession number GSE229402.

Acknowledgments

We thank John Cambier for his critical insight and editing of this manuscript.

This work was supported by grants from the National Institutes of Health (P30DK116073 [Lori Sussel], R03DK129925 [M.J. Smith], and K01OD63021764 [M.J. Smith]) and nPOD (Maki Nakayama). This research was performed with the support of the nPOD (RRID:SCR_014641), a collaborative T1D research project supported by JDRF (nPOD: 5-SRA-2018-557-Q-R), and the Leona M. & Harry B. Helmsley Charitable Trust (Grant#2018PG-T1D053, G-2108-04793). The content and views expressed are the responsibility of the authors and do not necessarily reflect the official view of nPOD. Organ procurement organizations partnering with nPOD to provide research resources are listed at http://www.jdrfnpod.org/for-partners/npod-partners/.

Author contributions: P.A. Gottlieb and M.J. Smith designed the research and reviewed and edited the manuscript; Z.C. Stensland, C.A. Magera, H. Broncucia, and M. Rihanek recruited subjects. M.J. Smith provided funding. Z.C. Stensland, B. Gomez, N. Rios-Guzman, C. Nicholas, and K. Toole performed experiments. Z.C. Stensland, K.W. Wells, and M.J. Smith analyzed the

data and prepared figures. H. Broncucia was the study coordinator. Z.C. Stensland, P.A. Gottlieb, and M.J. Smith wrote the manuscript.

Disclosures: The authors declare no competing interests exist.

Submitted: 15 September 2022
Revised: 15 March 2023
Accepted: 21 April 2023

References

Bingley, P.J., D.C. Boulware, J.P. Krischer, G. Type, and Type 1 Diabetes TrialNet Study Group. 2016. The implications of autoantibodies to a single islet antigen in relatives with normal glucose tolerance: Development of other autoantibodies and progression to type 1 diabetes. *Diabetologia*. 59: 542–549. https://doi.org/10.1007/s00125-015-3830-2

Calderon, D., M.L.T. Nguyen, A. Mezger, A. Kathiria, F. Müller, V. Nguyen, N. Lescano, B. Wu, J. Trombetta, J.V. Ribado, et al. 2019. Landscape of stimulation-responsive chromatin across diverse human immune cells. *Nat. Genet.* 51:1494–1505. https://doi.org/10.1038/s41588-019-0505-9

Cambier, J.C., S.B. Gauld, K.T. Merrell, and B.J. Vilen. 2007. B-Cell anergy: From transgenic models to naturally occurring anergic B cells? *Nat. Rev. Immunol.* 7:633–643. https://doi.org/10.1038/nri2133

Cowan, G.J.M., K. Miles, L. Capitani, S.S.B. Giguere, H. Johnsson, C. Goodyear, I.B. McInnes, S. Breusch, D. Gray, and M. Gray. 2020. In human autoimmunity, a substantial component of the B cell repertoire consists of polyclonal, barely mutated IgG^{+ve} B cells. *Front. Immunol.* 11:395. https://doi.org/10.3389/fimmu.2020.00395

Cyster, J.G., and C.C. Goodnow. 1995. Antigen-induced exclusion from follicles and anergy are separate and complementary processes that influence peripheral B cell fate. *Immunity*. 3:691–701. https://doi.org/10.1016/1074-7613(95)90059-4

Deng, C., Y. Xiang, T. Tan, Z. Ren, C. Cao, G. Huang, L. Wen, and Z. Zhou. 2016. Altered peripheral B-lymphocyte subsets in type 1 diabetes and latent autoimmune diabetes in adults. *Diabetes Care*. 39:434–440. https://doi.org/10.2337/dc15-1765

Dufort, M.J., C.J. Greenbaum, C. Speake, and P.S. Linsley. 2019. Cell type-specific immune phenotypes predict loss of insulin secretion in new-onset type 1 diabetes. *JCI Insight*. 4:e125556. https://doi.org/10.1172/jci.insight.125556

Duty, J.A., P. Szodoray, N.Y. Zheng, K.A. Koelsch, Q. Zhang, M. Swiatkowski, M. Mathias, L. Garman, C. Helms, B. Nakken, et al. 2009. Functional anergy in a subpopulation of naive B cells from healthy humans that express autoreactive immunoglobulin receptors. *J. Exp. Med.* 206: 139–151. https://doi.org/10.1084/jem.20080611

Falcone, M., J. Lee, G. Patstone, B. Yeung, and N. Sarvetnick. 1998. B lymphocytes are crucial antigen-presenting cells in the pathogenic autoimmune response to GAD65 antigen in nonobese diabetic mice. *J. Immunol.* 161:1163–1168. https://doi.org/10.4049/jimmunol.161.3.1163

Fu, R., A.E. Gillen, R.M. Sheridan, C. Tian, M. Daya, Y. Hao, J.R. Hesselberth, and K.A. Riemondy. 2020. clustifyr: an R package for automated single-cell RNA sequencing cluster classification. *F1000 Res.* 9:223. https://doi.org/10.12688/f1000research.22969.2

Fulcher, D.A., and A. Basten. 1994. Reduced life span of anergic self-reactive B cells in a double-transgenic model. *J. Exp. Med.* 179:125–134. https://doi.org/10.1084/jem.179.1.125

Gauld, S.B., R.J. Benschop, K.T. Merrell, and J.C. Cambier. 2005. Maintenance of B cell anergy requires constant antigen receptor occupancy and signaling. *Nat. Immunol.* 6:1160–1167. https://doi.org/10.1038/ni1256

Gauld, S.B., K.T. Merrell, and J.C. Cambier. 2006. Silencing of autoreactive B cells by anergy: A fresh perspective. *Curr. Opin. Immunol.* 18:292–297. https://doi.org/10.1016/j.coi.2006.03.015

Getahun, A., N.A. Beavers, S.R. Larson, M.J. Shlomchik, and J.C. Cambier. 2016. Continuous inhibitory signaling by both SHP-1 and SHIP-1 pathways is required to maintain unresponsiveness of anergic B cells. *J. Exp. Med.* 213:751–769. https://doi.org/10.1084/jem.20150537

Gorus, F.K., E.V. Balti, A. Messaaoui, S. Demeester, A. Van Dalem, O. Costa, H. Dorchy, C. Mathieu, L. Van Gaal, B. Keymeulen, et al. 2017. Twenty-year progression rate to clinical onset according to autoantibody profile, age, and HLA-DQ genotype in a registry-based group of children and adults with a first-degree relative with type 1 diabetes. *Diabetes Care*. 40: 1065–1072. https://doi.org/10.2337/dc16-2228

Hao, Y., S. Hao, E. Andersen-Nissen, W.M. Mauck III, S. Zheng, A. Butler, M.J. Lee, A.J. Wilk, C. Darby, M. Zager, et al. 2021. Integrated analysis of multimodal single-cell data. *Cell*. 184:3573–3587.e29. https://doi.org/10.1016/j.cell.2021.04.048

Hong, R., N. Lai, R. Ouchida, E. Xiong, Y. Zhou, Q. Min, J. Liu, Y. Tang, M. Hikida, T. Tsubata, et al. 2019. The B cell novel protein 1 (BCNP1) regulates BCR signaling and B cell apoptosis. *Eur. J. Immunol.* 49:911–917. https://doi.org/10.1002/eji.201847985

Inoue, Y., T. Kaifu, A. Sugahara-Tobinai, A. Nakamura, J. Miyazaki, and T. Takai. 2007. Activating Fc gamma receptors participate in the development of autoimmune diabetes in NOD mice. *J. Immunol.* 179:764–774. https://doi.org/10.4049/jimmunol.179.2.764

Jahnmatz, M., G. Kesa, E. Netterlid, A.M. Buisman, R. Thorstensson, and N. Ahlborg. 2013. Optimization of a human IgG B-cell ELISpot assay for the analysis of vaccine-induced B-cell responses. *J. Immunol. Methods*. 391: 50–59. https://doi.org/10.1016/j.jim.2013.02.009

Jenks, S.A., K.S. Cashman, E. Zumaquero, U.M. Marigorta, A.V. Patel, X. Wang, D. Tomar, M.C. Woodruff, Z. Simon, R. Bugrovsky, et al. 2018. Distinct effector B cells induced by unregulated toll-like receptor 7 contribute to pathogenic responses in systemic lupus erythematosus. *Immunity*. 49:725–739.e6. https://doi.org/10.1016/j.immuni.2018.08.015

Kleffel, S., A. Vergani, S. Tezza, M. Ben Nasr, M.A. Niewczas, S. Wong, R. Bassi, F. D'Addio, T. Schatton, R. Abdi, et al. 2015. Interleukin-10+ regulatory B cells arise within antigen-experienced CD40+ B cells to maintain tolerance to islet autoantigens. *Diabetes*. 64:158–171. https://doi.org/10.2337/db13-1639

Koelsch, K., N.Y. Zheng, Q. Zhang, A. Duty, C. Helms, M.D. Mathias, M. Jared, K. Smith, J.D. Capra, and P.C. Wilson. 2007. Mature B cells class switched to IgD are autoreactive in healthy individuals. *J. Clin. Invest.* 117:1558–1565. https://doi.org/10.1172/JCI27628

Leete, P., A. Willcox, L. Krogvold, K. Dahl-Jørgensen, A.K. Foulis, S.J. Richardson, and N.G. Morgan. 2016. Differential insulitic profiles determine the extent of β-cell destruction and the age at onset of type 1 diabetes. *Diabetes*. 65:1362–1369. https://doi.org/10.2337/db15-1615

Lighvani, A.A., D.M. Frucht, D. Jankovic, H. Yamane, J. Aliberti, B.D. Hissong, B.V. Nguyen, M. Gadina, A. Sher, W.E. Paul, and J.J. O'Shea. 2001. T-bet is rapidly induced by interferon-gamma in lymphoid and myeloid cells. *Proc. Natl. Acad. Sci. USA*. 98:15137–15142. https://doi.org/10.1073/pnas.261570598

McGinnis, C.S., L.M. Murrow, and Z.J. Gartner. 2019. DoubletFinder: Doublet detection in single-cell RNA sequencing data using artificial nearest Neighbors. *Cell Syst.* 8:329–337.e4. https://doi.org/10.1016/j.cels.2019.03.003

Moura, R.A., C. Quaresma, A.R. Vieira, M.J. Gonçalves, J. Polido-Pereira, V.C. Romão, N. Martins, H. Canhão, and J.E. Fonseca. 2017. B-cell phenotype and IgD-CD27- memory B cells are affected by TNF-inhibitors and tocilizumab treatment in rheumatoid arthritis. *PLoS One*. 12:e0182927. https://doi.org/10.1371/journal.pone.0182927

Mulè, M.P., A.J. Martins, and J.S. Tsang. 2022. Normalizing and denoising protein expression data from droplet-based single cell profiling. *Nat. Commun.* 13:2099. https://doi.org/10.1038/s41467-022-29356-8

Pignarre, A., F. Chatonnet, G. Caron, M. Haas, F. Desmots, and T. Fest. 2021. Plasmablasts derive from CD23- activated B cells after the extinction of IL-4/STAT6 signaling and IRF4 induction. *Blood*. 137:1166–1180. https://doi.org/10.1182/blood.2020005083

Pinna, D., D. Corti, D. Jarrossay, F. Sallusto, and A. Lanzavecchia. 2009. Clonal dissection of the human memory B-cell repertoire following infection and vaccination. *Eur. J. Immunol.* 39:1260–1270. https://doi.org/10.1002/eji.200839129

Powell, W.E., S.J. Hanna, C.N. Hocter, E. Robinson, J. Davies, G.J. Dunseath, S. Luzio, D. Farewell, L. Wen, C.M. Dayan, et al. 2018. Loss of CXCR3 expression on memory B cells in individuals with long-standing type 1 diabetes. *Diabetologia*. 61:1794–1803. https://doi.org/10.1007/s00125-018-4651-x

Racine, R., M. Chatterjee, and G.M. Winslow. 2008. CD11c expression identifies a population of extrafollicular antigen-specific splenic plasmablasts responsible for CD4 T-independent antibody responses during intracellular bacterial infection. *J. Immunol.* 181:1375–1385. https://doi.org/10.4049/jimmunol.181.2.1375

Richardson, C., A.S. Chida, D. Adlowitz, L. Silver, E. Fox, S.A. Jenks, E. Palmer, Y. Wang, J. Heimburg-Molinaro, Q.Z. Li, et al. 2013. Molecular basis of 9G4 B cell autoreactivity in human systemic lupus erythematosus. *J. Immunol.* 191:4926–4939. https://doi.org/10.4049/jimmunol.1202263

Roep, B.O., F.S. Kleijwegt, A.G. van Halteren, V. Bonato, U. Boggi, F. Vendrame, P. Marchetti, and F. Dotta. 2010. Islet inflammation and CXCL10 in recent-onset type 1 diabetes. *Clin. Exp. Immunol.* 159:338–343. https://doi.org/10.1111/j.1365-2249.2009.04087.x

Rubtsov, A.V., K. Rubtsova, A. Fischer, R.T. Meehan, J.Z. Gillis, J.W. Kappler, and P. Marrack. 2011. Toll-like receptor 7 (TLR7)-driven accumulation of a novel CD11c^{+} B-cell population is important for the development of autoimmunity. *Blood*. 118:1305–1315. https://doi.org/10.1182/blood-2011-01-331462

Saadoun, D., B. Terrier, J. Bannock, T. Vazquez, C. Massad, I. Kang, F. Joly, M. Rosenzwajg, D. Sene, P. Benech, et al. 2013. Expansion of autoreactive unresponsive CD21-/low B cells in Sjögren's syndrome-associated lymphoproliferation. *Arthritis Rheum.* 65:1085–1096. https://doi.org/10.1002/art.37828

Sarkar, S.A., C.E. Lee, F. Victorino, T.T. Nguyen, J.A. Walters, A. Burrack, J. Eberlein, S.K. Hildemann, and D. Homann. 2012. Expression and regulation of chemokines in murine and human type 1 diabetes. *Diabetes*. 61:436–446. https://doi.org/10.2337/db11-0853

Serreze, D.V., S.A. Fleming, H.D. Chapman, S.D. Richard, E.H. Leiter, and R.M. Tisch. 1998. B lymphocytes are critical antigen-presenting cells for the initiation of T cell-mediated autoimmune diabetes in nonobese diabetic mice. *J. Immunol.* 161:3912–3918. https://doi.org/10.4049/jimmunol.161.8.3912

Silva, D.G., S.R. Daley, J. Hogan, S.K. Lee, C.E. Teh, D.Y. Hu, K.P. Lam, C.C. Goodnow, and C.G. Vinuesa. 2011. Anti-islet autoantibodies trigger autoimmune diabetes in the presence of an increased frequency of islet-reactive CD4 T cells. *Diabetes*. 60:2102–2111. https://doi.org/10.2337/db10-1344

Silveira, P.A., E. Johnson, H.D. Chapman, T. Bui, R.M. Tisch, and D.V. Serreze. 2002. The preferential ability of B lymphocytes to act as diabetogenic APC in NOD mice depends on expression of self-antigen-specific immunoglobulin receptors. *Eur. J. Immunol.* 32:3657–3666. https://doi.org/10.1002/1521-4141(200212)32:12<3657::AID-IMMU3657>3.0.CO;2-E

Smith, M.J., B.R. Ford, M. Rihanek, B.M. Coleman, A. Getahun, V.D. Sarapura, P.A. Gottlieb, and J.C. Cambier. 2019. Elevated PTEN expression maintains anergy in human B cells and reveals unexpectedly high repertoire autoreactivity. *JCI Insight*. 4:e123384. https://doi.org/10.1172/jci.insight.123384

Smith, M.J., T.A. Packard, S.K. O'Neill, C.J. Henry Dunand, M. Huang, L. Fitzgerald-Miller, D. Stowell, R.M. Hinman, P.C. Wilson, P.A. Gottlieb, and J.C. Cambier. 2015. Loss of anergic B cells in prediabetic and new-onset type 1 diabetic patients. *Diabetes*. 64:1703–1712. https://doi.org/10.2337/db13-1798

Smith, M.J., R.M. Hinman, A. Getahun, S. Kim, T.A. Packard, and J.C. Cambier. 2018a. Silencing of high-affinity insulin-reactive B lymphocytes by anergy and impact of the NOD genetic background in mice. *Diabetologia*. 61:2621–2632. https://doi.org/10.1007/s00125-018-4730-z

Smith, M.J., M. Rihanek, C. Wasserfall, C.E. Mathews, M.A. Atkinson, P.A. Gottlieb, and J.C. Cambier. 2018b. Loss of B-cell anergy in type 1 diabetes is associated with high-risk HLA and non-HLA disease susceptibility alleles. *Diabetes*. 67:697–703. https://doi.org/10.2337/db17-0937

Smith, M.J., K.M. Simmons, and J.C. Cambier. 2017. B cells in type 1 diabetes mellitus and diabetic kidney disease. *Nat. Rev. Nephrol.* 13:712–720. https://doi.org/10.1038/nrneph.2017.138

Speake, C., S.O. Skinner, D. Berel, E. Whalen, M.J. Dufort, W.C. Young, J.M. Odegard, A.M. Pesenacker, F.K. Gorus, E.A. James, et al. 2019. A composite immune signature parallels disease progression across T1D subjects. *JCI Insight*. 4:e126917. https://doi.org/10.1172/jci.insight.126917

Steck, A.K., F. Dong, K. Waugh, B.I. Frohnert, L. Yu, J.M. Norris, and M.J. Rewers. 2016. Predictors of slow progression to diabetes in children with multiple islet autoantibodies. *J. Autoimmun.* 72:113–117. https://doi.org/10.1016/j.jaut.2016.05.010

Steck, A.K., K. Johnson, K.J. Barriga, D. Miao, L. Yu, J.C. Hutton, G.S. Eisenbarth, and M.J. Rewers. 2011. Age of islet autoantibody appearance and mean levels of insulin, but not GAD or IA-2 autoantibodies, predict age of diagnosis of type 1 diabetes: Diabetes autoimmunity study in the young. *Diabetes Care*. 34:1397–1399. https://doi.org/10.2337/dc10-2088

Stensland, Z.C., and M.J. Smith. 2021. Enrichment and detection of antigen-binding B cells for mass cytometry. *Magnetochemistry*. 7:92. https://doi.org/10.3390/magnetochemistry7070092

Thompson, W.S., M.L. Pekalski, H.Z. Simons, D.J. Smyth, X. Castro-Dopico, H. Guo, C. Guy, D.B. Dunger, S. Arif, M. Peakman, et al. 2014. Multiparametric flow cytometric and genetic investigation of the peripheral B cell compartment in human type 1 diabetes. *Clin. Exp. Immunol.* 177:571–585. https://doi.org/10.1111/cei.12362

Tipton, C.M., C.F. Fucile, J. Darce, A. Chida, T. Ichikawa, I. Gregoretti, S. Schieferl, J. Hom, S. Jenks, R.J. Feldman, et al. 2015. Diversity, cellular origin and autoreactivity of antibody-secreting cell population expansions in acute systemic lupus erythematosus. *Nat. Immunol.* 16:755–765. https://doi.org/10.1038/ni.3175

Tough, D.F., and J. Sprent. 1995. Lifespan of lymphocytes. *Immunol. Res.* 14:1–12. https://doi.org/10.1007/BF02918494

Uno, S., A. Imagawa, K. Saisho, K. Okita, H. Iwahashi, T. Hanafusa, and I. Shimomura. 2010. Expression of chemokines, CXC chemokine ligand 10 (CXCL10) and CXCR3 in the inflamed islets of patients with recent-onset autoimmune type 1 diabetes. *Endocr. J.* 57:991–996. https://doi.org/10.1507/endocrj.K10E-076

Wong, F.S., L. Wen, M. Tang, M. Ramanathan, I. Visintin, J. Daugherty, L.G. Hannum, C.A. Janeway Jr, and M.J. Shlomchik. 2004. Investigation of the role of B-cells in type 1 diabetes in the NOD mouse. *Diabetes*. 53:2581–2587. https://doi.org/10.2337/diabetes.53.10.2581

Zheng, G.X., J.M. Terry, P. Belgrader, P. Ryvkin, Z.W. Bent, R. Wilson, S.B. Ziraldo, T.D. Wheeler, G.P. McDermott, J. Zhu, et al. 2017. Massively parallel digital transcriptional profiling of single cells. *Nat. Commun.* 8:14049. https://doi.org/10.1038/ncomms14049

JEM

Supplemental material

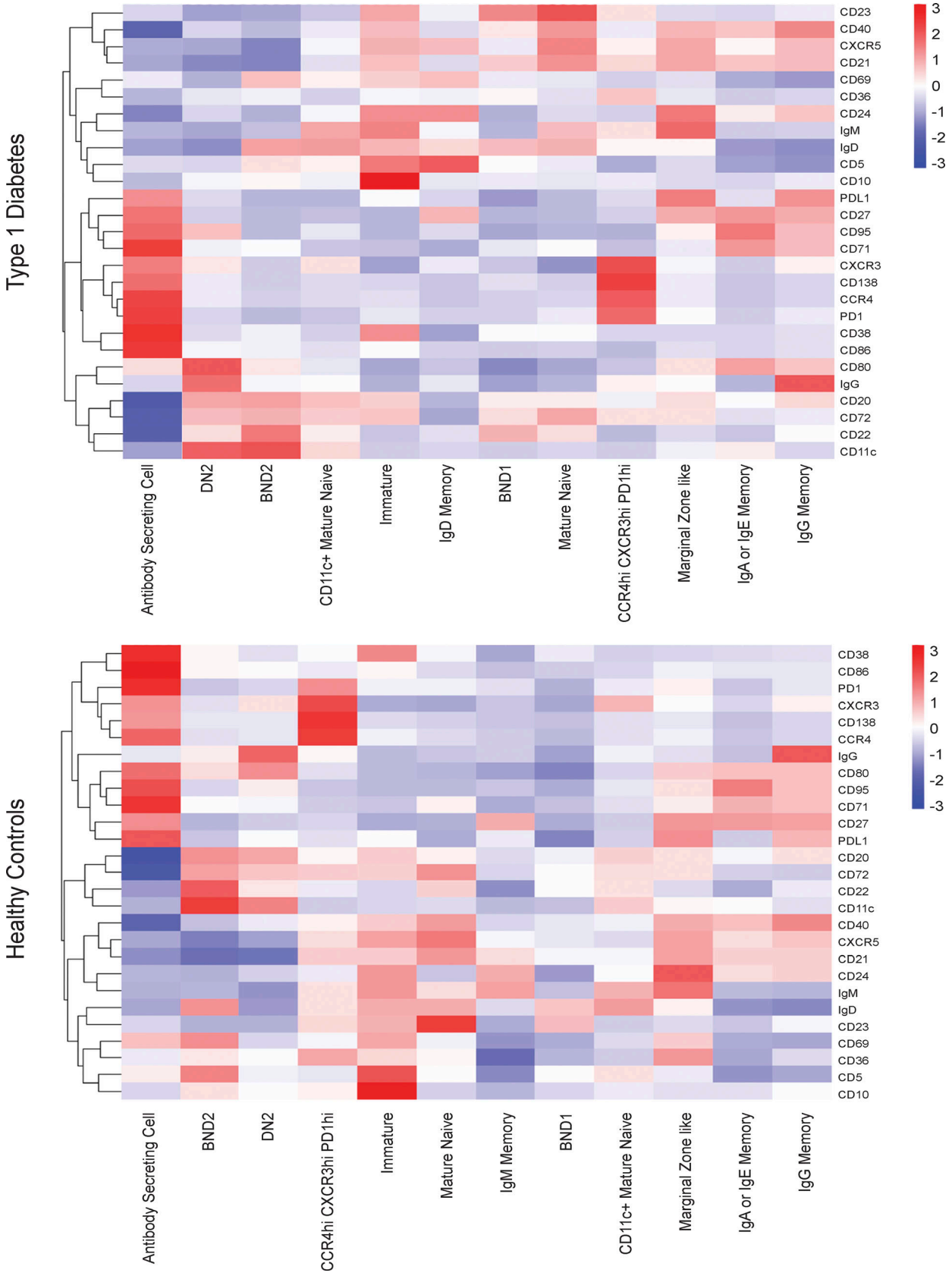

Figure S1. **Heatmap of surface marker expression levels in the B cell subsets identified by unsupervised clustering for T1D and HC donors.**

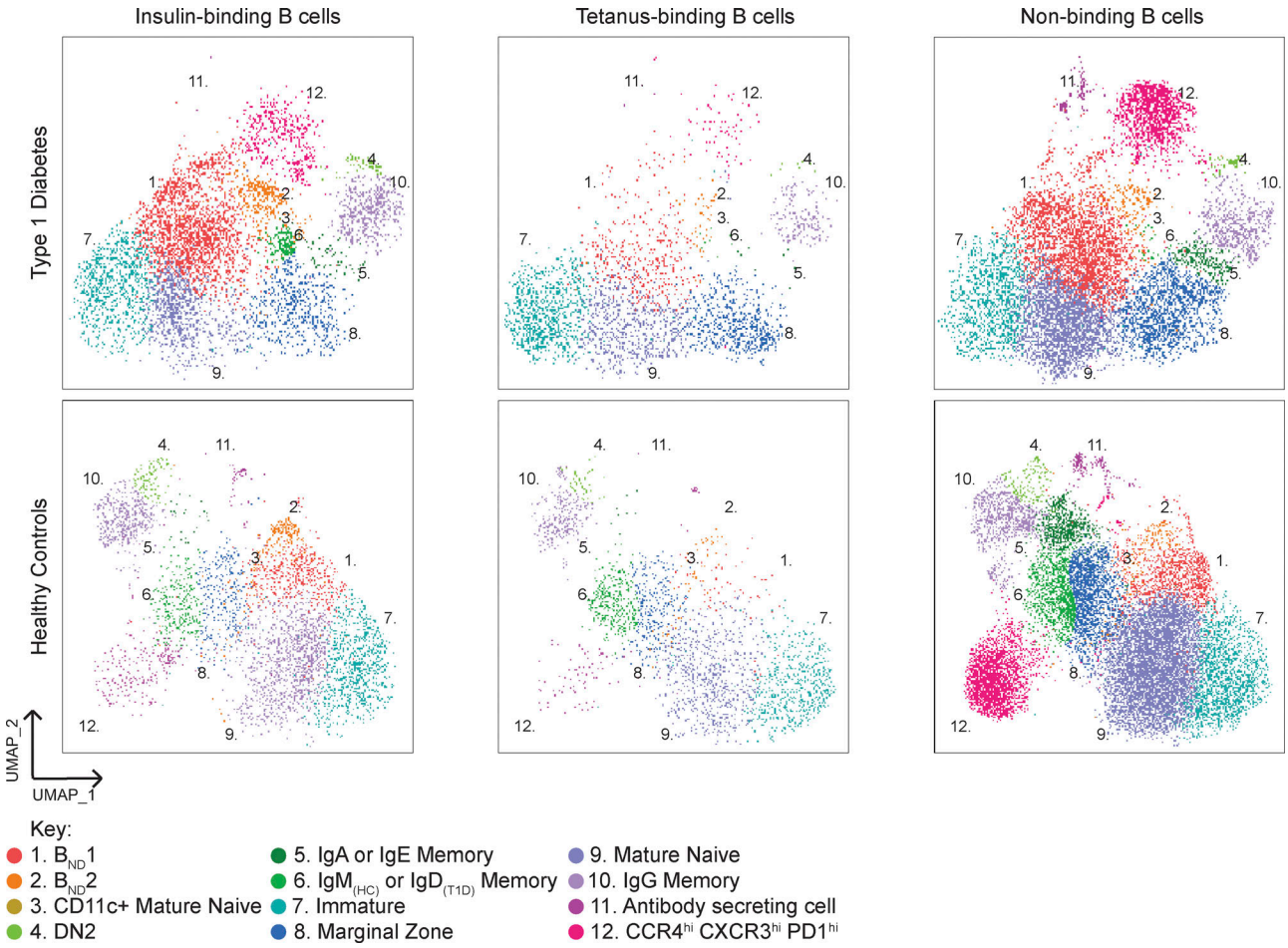

Figure S2. **UMAP projections for insulin-binding-only, tetanus-binding-only, and non-binding-only B cells from T1D and HC donors.**

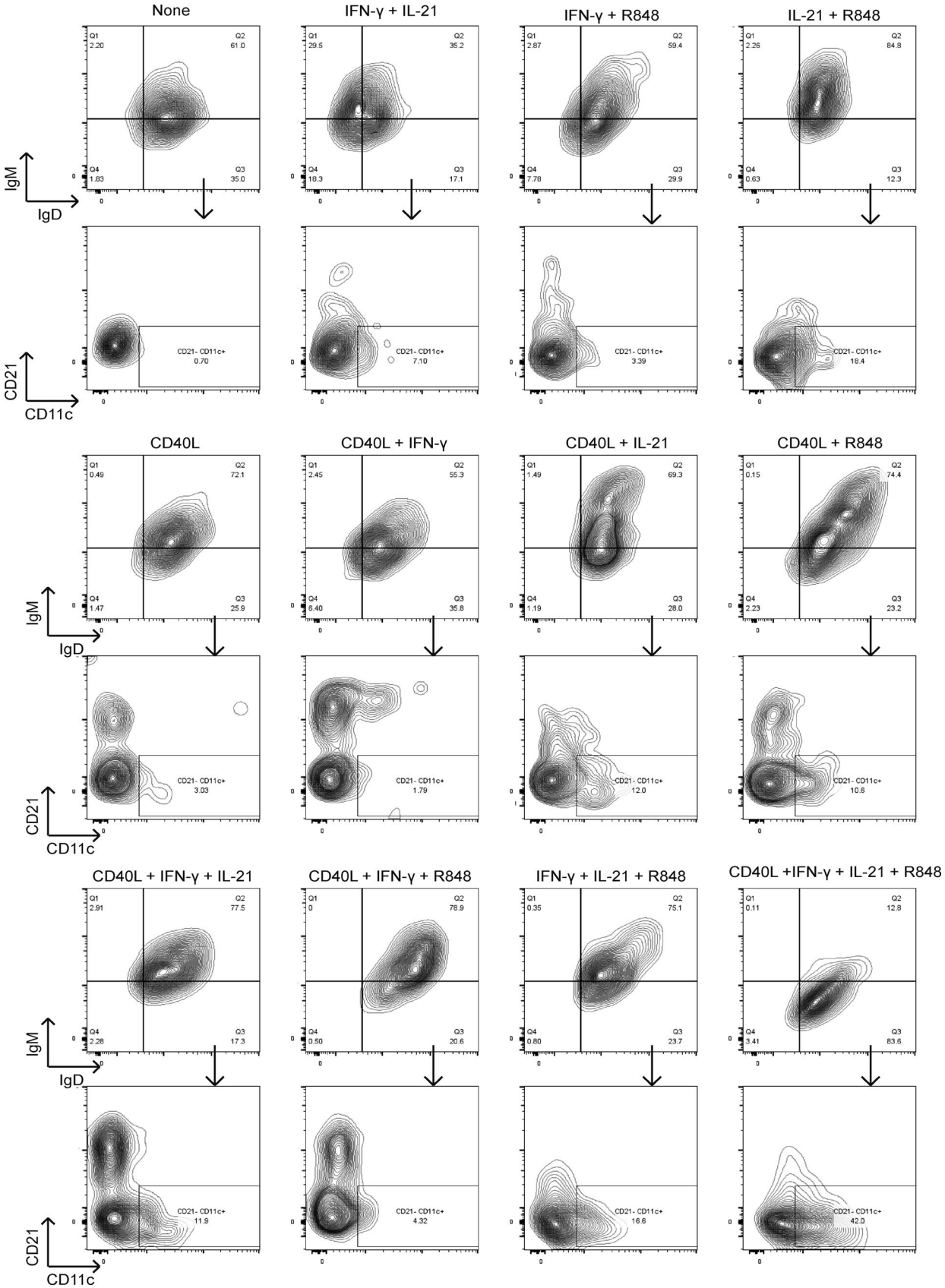

Figure S3. **Cytograms of B cell phenotype of $B_{ND}1$ cells after stimulation with the indicated reagents after 5 d.** The majority of $B_{ND}1$ ($CD19^+$ $CD27^-$ IgM^{lo} IgD^+ $CD21^+$ $CD11c^-$) cells revert to an MN B cell phenotype ($CD19^+$ $CD27^-$ IgM^+ IgD^+) after stimulation. A combination of CD40L, IFN-γ, IL-21, and R848 provide the best signals to maintain a B_{ND} phenotype and drive differentiation of $B_{ND}1$ cells into $B_{ND}2$ ($CD19^+$ $CD27^-$ IgM^{lo} IgD^+ $CD21^-$ $CD11c^+$) cells.

Provided online are two tables. Table S1 shows CyTOF antibody panel used in this study. Table S2 shows patient demographics and clinical information used in this study.